MroQ is a novel Abi-domain protein that influences virulence gene expression in *Staphylococcus aureus* via modulation of agr activity

By: Stephanie Marroquin, Brittney Gimza, Brooke Tomlinson, Michelle Stein, Andrew Frey, Rebecca A. Keogh, Rachel Zapf, Daniel A. Todd, Nadja B. Cech, Ronan K. Carroll, and Lindsey N. Shaw

Marroquin, Stephanie; Gimza, Brittney; Tomlinson, Brooke; Stein, Michelle; Frey, Andrew; Keogh, Rebecca A.; Zapf, Rachel; Todd, Daniel A.; Cech, Nadja B.; Carroll, Ronan K.; Shaw, Lindsey N. (2019). MroQ is a novel Abi-domain protein that influences virulence gene expression in Staphylococcus aureus via modulation of agr activity. *Infection and Immunity* *87*(5), e00002-19. https://doi.org/10.1128/IAI.00002-19

Abstract:

Numerous factors have, to date, been identified as playing a role in the regulation of Agr activity in *Staphylococcus aureus*, including transcription factors, antisense RNAs, and host elements. Herein we investigated the product of SAUSA300_1984 (termed MroQ), a transmembrane Abi-domain/M79 protease-family protein, as a novel effector of this system. Using a USA300 *mroQ* mutant, we observed a drastic reduction in proteolysis, hemolysis, and pigmentation that was fully complementable. This appears to result from diminished *agr* activity, as transcriptional analysis revealed significant decreases in expression of both RNAII and RNAIII in the *mroQ* mutant. Such effects appear to be direct, rather than indirect, as known *agr* effectors demonstrated limited alterations in their activity upon *mroQ* disruption. A comparison of RNA sequencing data sets for both *mroQ* and *agr* mutants revealed a profound overlap in their regulomes, with the majority of factors affected being known virulence determinants. Importantly, the preponderance of alterations in expression were more striking in the *agr* mutant, indicating that MroQ is necessary, but not sufficient, for Agr function. Mechanism profiling revealed that putative residues for metalloprotease activity within MroQ are required for its Agr-controlling effect; however, this was not wielded at the level of AgrD processing. Virulence assessment demonstrated that both *mroQ* and *agr* mutants exhibited increased formation of renal abscesses but decreased skin abscess formation alongside diminished dermonecrosis. Collectively, we present the characterization of a novel *agr* effector in *S. aureus* which would appear to be a direct regulator, potentially functioning via interaction with the AgrC histidine kinase.

Keywords: MRSA | Staphylococcus aureus | transcriptional regulation | virulence factor

Article:

INTRODUCTION

Pathogenicity in *Staphylococcus aureus* is both diverse and tightly controlled, being highly adaptive to the surrounding environment and available resources (1). In order to survive and persist within the host, this pathogen produces a wide array of virulence factors throughout the different stages of infection (2). For example, during earlier phases of growth, adhesins and other binding proteins are actively synthesized (e.g., Spa, FnbAB) and play a role in colonization (2, 3). In contrast, in later phases, these surface proteins are repressed, while secreted toxins, proteases, and exoenzymes are produced to facilitate invasion and dissemination (2, 4). This coordination is facilitated by an array of global regulators of gene expression (2, 5–10).

The *agr* quorum-sensing system is one of the most important regulators of virulence in *S. aureus* (11). It is a quorum-sensing system comprised of two transcriptional units, RNAII and RNAIII, each controlled by its own promoter, P2 and P3, respectively. RNAII encodes the *agr* operon, which is comprised of four genes, *agrBDCA* (12). The quorum-sensing system functions in three parts: (i) a quorum-sensing module comprised of AgrB and AgrD, (ii) a two-component system (TCS) consisting of AgrC and AgrA, and (iii) an effector molecule, termed RNAIII, which serves as a regulatory RNA (2, 12, 13). The pheromone for the *agr* system is known as autoinducing peptide (AIP) and is a derivative of the AgrD polypeptide. In order to reach its active form (AIP), AgrD is initially processed by AgrB, a multifunctional endopeptidase that also acts as a chaperone, followed by processing by the SpsB signal peptidase (14, 15). AIP is exported by AgrB and accumulates extracellularly until a threshold is reached, when it binds AgrC, the histidine kinase (HK) of the TCS. This leads to autophosphorylation of the protein (12, 16), followed by transfer of that phosphate to AgrA, the cytoplasmic response regulator (RR) (15). Upon activation, AgrA directly binds to the P2 and P3 promoters, upregulating expression of RNAII, as a positive feedback loop, as well as RNAIII (12). RNAIII subsequently modulates the expression of an assortment of genes involved in virulence, thus exerting the crucial role of *agr* in *S. aureus* pathogenesis. To date, numerous regulators of *agr* have been identified (5, 7, 8, 17–21), including transcription factors, such as SarR and CodY (5, 20); antisense RNAs, such as the *psm-mec* RNA transcript (22); and host factors, such as the serum protein apolipoprotein B (23).

Abi proteins have previously been noted to play a protective role against viral infection by halting cellular activity in infected bacterial cells, so as to prevent further replication of the invading bacteriophage (24). These proteins are also members of the M79 metalloprotease family, which in eukaryotes are also noted as CAAX prenyl proteases (25, 26). These eukaryotic proteases are involved in posttranslational modification through a mechanism known as prenylation, where the AAX motif of target proteins is cleaved from the C terminus by M79 enzymes, followed by the addition of an isoprenoid on the remaining cysteine residue (27). Work by our group exploring the prenylation process in bacteria has demonstrated that the C-terminal CAAX motif is present in only a few proteins, suggesting that this mechanism is not conserved in prokaryotes (28). Indeed, only a single protein has been shown to be prenylated in bacteria: ComX from *Bacillales* species is known to be prenylated at a conserved C-terminal tryptophan residue (29), although it is not known if proteolysis is a requirement for this event.

Beyond a role in protecting against phage infection, Abi proteins have been characterized in only two other studies. The first, Abx1, has been the subject of study in group B streptococci (27). Notably, an *abx1* mutant demonstrated a significant decrease in hemolytic activity and pigment

production, which was mediated via increased CovSR activity (27). In this work, Abx1 was shown to positively regulate CovS, a histidine kinase involved in virulence gene regulation, by forming a signaling complex. Moreover, the interaction was established to be direct, via the two CovS transmembrane domains, but not dependent on Abx1 proteolytic activity (27). More recently, an Abi-domain protein in *S. aureus*, SpdC, was characterized and shown to interact with the histidine kinase of the WalKR two-component system, which is involved in controlling cell wall metabolism (30). SpdC was also shown to interact with other histidine kinases, including SaeS, ArlS, and VraS, through interaction between transmembrane domains (30). Of note, although it is an Abi protein, SpdC lacks the conserved catalytic residues of M79 enzymes, and therefore it is a nonpeptidase homolog. As such, although they are still relatively underexplored, it is becoming increasingly apparent that Abi proteins in prokaryotes possess important regulatory functions that are seemingly mediated through interaction with the histidine kinase modules of two-component systems (27, 30).

In *S. aureus*, beyond SpdC, there are 5 other Abi-domain proteins encoded within the genome. Herein, we investigate the function of one of these, SAUSA300_1984, which is encoded by a region located upstream of the *agr* operon and which we name MroQ. We show that mutation of *mroQ* results in the decreased expression and abundance of secreted proteases, hemolysins, and toxins, as well as the increased production of surface-associated proteins. These effects were shown to be *agr* dependent, with the *mroQ* mutant demonstrating decreased expression of both RNAII and RNAIII. Importantly, known regulators of *agr* demonstrated limited alterations in transcription, potentially indicating a direct role for MroQ in controlling *agr* activity. We also noted decreased pigment production and enhanced biofilm formation in the *mroQ* mutant, which mirrored that of an *agr* mutant. Finally, we observed a decreased bacterial burden and dermonecrosis for *mroQ* mutant-infected mice using a model of skin abscess formation. Collectively, we present the characterization of a novel *agr* effector in *S. aureus*, which would appear to be a direct regulator, potentially functioning via interaction with the AgrC HK component.

RESULTS

MroQ serves to control protease production in *S. aureus*. Given the Shaw laboratory's long-standing interest in *S. aureus* secreted proteases, we screened the Nebraska Transposon Mutant Library (NTML) (31) for novel factors that could regulate their production. Using this mutant collection and casein agar plates, we identified an insertion in the gene *SAUSA300_1984* (hereafter named *mroQ*, for membrane protease regulator of Agr quorum sensing) that elicited a profound reduction in secreted protease activity (Fig. 1A). To explore this more broadly, we next analyzed proteolytic activity through gelatin zymography (Fig. 1B). Here, the *mroQ* mutant demonstrated a substantial decrease in the levels of multiple secreted proteases, which was rescued upon complementation in *trans*; indeed, complementation with a multicopy plasmid actually led to an increase in the production of secreted proteases in comparison to that in our wild-type strain. Next, to determine if the influence of MroQ on protease production was a consequence of modulated activity or altered transcription, we used a reporter gene fusion for the protease aureolysin. When this fusion was transduced into the USA300 wild type and *mroQ* mutant, we observed a significant impairment in aureolysin transcription in the mutant strain (Fig. 1C), thus indicating that the effects are wielded at the level of gene expression.

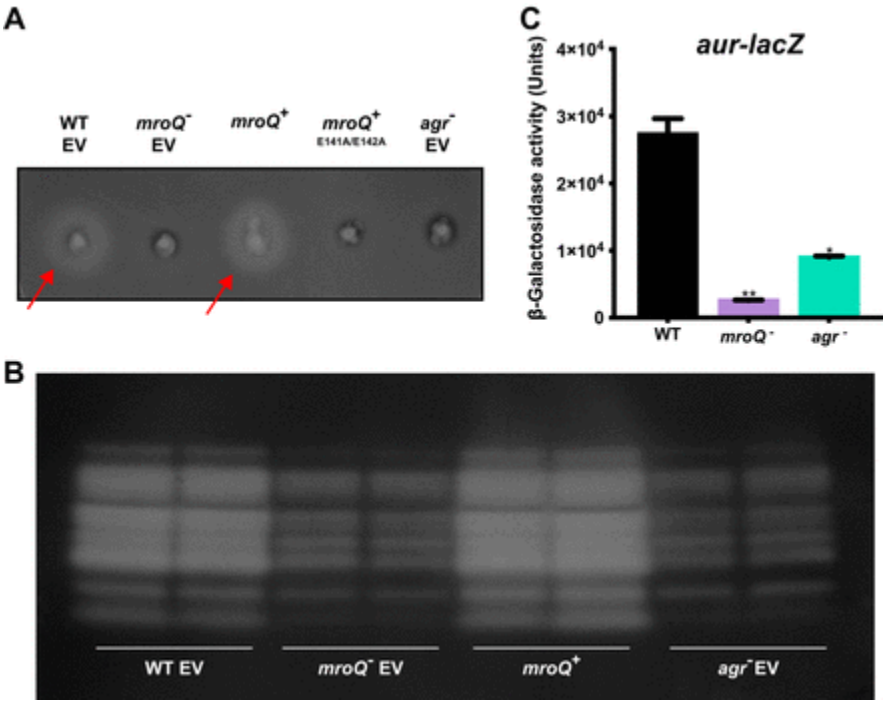

FIGURE 1. Disruption of *mroQ* results in diminished proteolytic activity in *S. aureus*. (A) The wild type (WT), *mroQ* mutant (*mroQ*$^-$), *mroQ*-complemented strain (*mroQ*$^+$), *mroQ* site-directed mutant (E141A/E142A)-complemented strain (*mroQ*$^-$ E141A/E142A), and *agr* mutant strain (*agr*$^-$) were plated on casein nutrient agar to observe changes in proteolysis. Red arrows highlight zones of proteolysis. (B) Gelatin zymography of the indicated strains. Note that white zones of clearing indicate proteolysis of the gelatin substrate. (C) Activity of an *aur-lacZ* fusion in the wild-type, *mroQ* mutant, and *agr* mutant strains. Data are from 4 h of growth, which is a peak window of aureolysin expression. Student's *t* test was used to determine statistical significance. *, $P < 0.05$; **, $P < 0.01$. Error bars show the SEM. EV, empty vector.

MroQ regulates the production of a wealth of *S. aureus* virulence determinants. To determine if the observed effects were specific to proteases, we next explored whether the production of other virulence factors was influenced by MroQ. Using a blood agar plate, we observed a significant decrease in hemolytic activity for the mutant strain compared to that for the wild type (Fig. 2A) that was restored upon complementation in *trans*. This activity was explored quantitatively using a hemolysin assay with whole human blood, revealing a substantial decrease in the ability of the mutant to lyse human erythrocytes, which was again complementable (Fig. 2B). To assess whether this effect was mediated at the transcriptional level, we used a reporter gene fusion for the primary hemolysin in *S. aureus*, *hla*. When the activity of this construct was assessed between the wild type and the *mroQ*-null strain, we observed a significant decrease in the mutant, indicating that these effects are also mediated at the level of gene expression (Fig. 2C). To further investigate the role of MroQ and its influence on other virulence determinants, we performed a Western blot analysis for the Panton-Valentine leukocidin (PVL) toxin and the surface-exposed virulence factor surface protein A (Spa). Upon analysis we determined that PVL was highly abundant in the wild type and the *mroQ*-complemented strain; however, it was entirely absent in the *mroQ* mutant (Fig. 2D). Conversely, in blots with Spa, we found an increased abundance in the *mroQ* mutant, whereas we noted an

absence in the wild type and the *mroQ*-complemented strain (Fig. 2E). To ensure that these substantial changes in virulence factor production were not the result of a simple growth defect in the mutant, we measured cell density over time. We found no significant difference when performing these studies between the wild-type, mutant and complemented strains (data not shown).

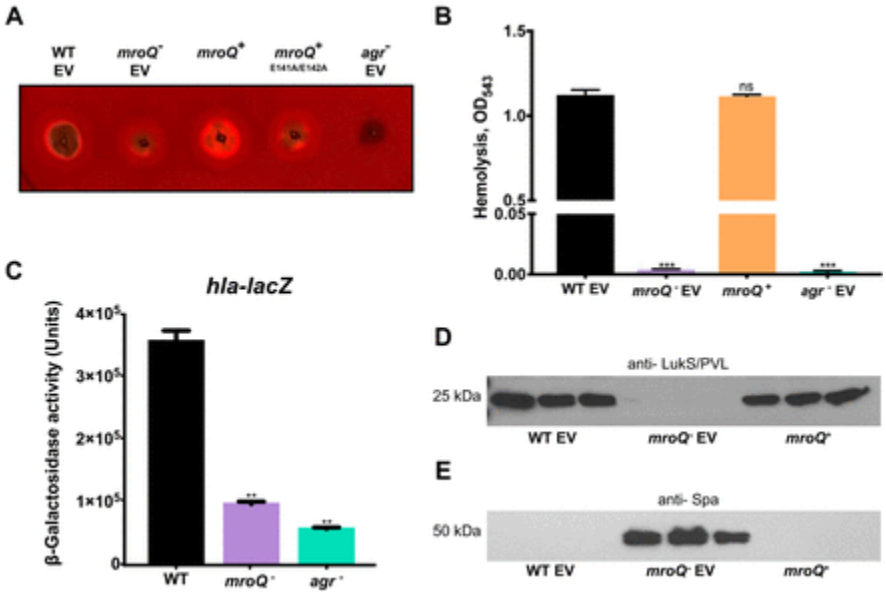

FIGURE 2. MroQ globally regulates virulence factor production in *S. aureus*. (A) The wild type, *mroQ* mutant, *mroQ*-complemented strain, *mroQ* site-directed mutant (E141A/E142A)-complemented strain and *agr* mutant strain were plated on sheep blood agar to observe changes in hemolysis. (B) Hemolytic activity was measured via lysis of erythrocytes in whole human blood. (C) Activity of an *hla-lacZ* fusion in the wild-type, *mroQ* mutant, and *agr* mutant strains. Data are from 4 h of growth, which is a peak window of alpha-hemolysin expression. (D, E) Immunoblots for abundance of the LukS component of the Panton-Valentine leukocidin (PVL) (D) and surface protein A (SpA) (E) in the wild-type, *mroQ* mutant, and complemented strains. Student's *t* test was used to determine statistical significance. **, $P < 0.01$; ***, $P < 0.001$; ns, not significant. Error bars show the SEM. EV, empty vector.

MroQ mediates its effects via modulation of *agr* activity in *S. aureus*. Our findings thus far for the *mroQ* mutant are in line with those which one might expect for a strain exhibiting altered activity of the central virulence factor regulator, *agr*. Indeed, when we repeated our proteolysis and hemolysis activity and transcription studies whose results are presented in Fig. 1 and 2 with an *agr* mutant strain, we saw results very similar to those obtained with the *mroQ* mutant. As such, we next sought to assess changes in promoter activity for the *agr* P2 and P3 promoters in the *mroQ* mutant using quantitative real-time PCR (qPCR) analysis (Fig. 3). When the abundance of the RNAII (Fig. 3A) and RNAIII (Fig. 3B) gene transcripts was measured, we observed a marked decrease for both transcripts in the mutant compared to the parent. Specifically, the activity from the P2 promoter was decreased by 15.6-fold, while the activity from the P3 promoter was decreased a striking 292-fold.

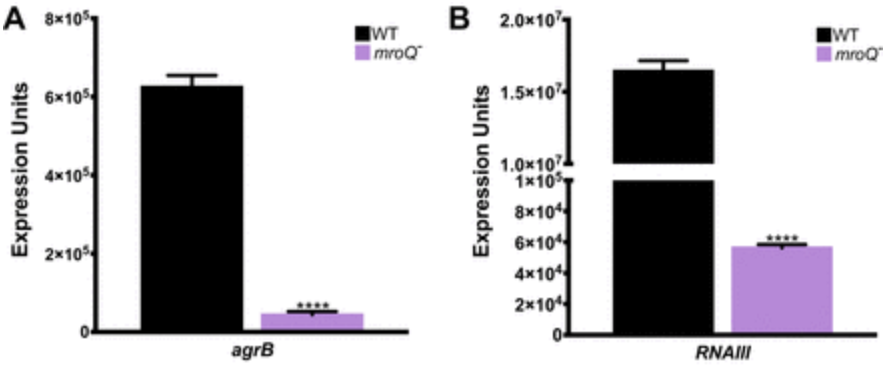

FIGURE 3. The RNAII and RNAIII genes are significantly downregulated upon *mroQ* disruption. qPCR was performed on the *mroQ* mutant and USA300 wild-type strains grown in TSB to late exponential phase. Target expression levels were normalized to the 16S rRNA expression level. *agrB* was used as a measure of RNAII gene transcript abundance (A), and RNAIII was examined for transcript abundance (B). Student's *t* test was used to determine statistical significance. ****, $P \leq 0.0001$. Error bars show the SEM.

To further clarify these effects, we next assessed the transcription of a range of genes downstream of *agr* whose transcription is dependent on its activity. Here, some very notable changes in expression between the wild type and the mutant were observed, including the expression of numerous genes involved in virulence that are positively regulated by *agr*. Specifically, decreases in the mutant strain were observed for *psmα1* (2,666-fold), *sspA* (57.3-fold), *lukS-PV* (35.4-fold), and *lip* (132.2-fold). Further, the notable regulator *saeR*, which is positively influenced by the *agr* system, demonstrated a 3.8-fold decrease in transcription in the mutant. Additionally, *spa*, which is repressed by the *agr* effector RNAIII, demonstrated a 792-fold increase in transcription in the mutant, as did the notable SarA homolog *sarS* (which is also negatively regulated by *agr*), which was found to have a 2.1-fold increase in transcription. Another surface protein that is repressed by RNAIII, *sdrD*, also demonstrated a 2.7-fold increase in transcription in the mutant strain (Fig. 4).

To determine if these were likely direct or indirect effects, we next sought to measure the expression of a cadre of known upstream effectors of the *agr* system. Accordingly, expression of positive (*sarA*, *sarZ*, *sarU*, and *mgrA*) and negative (*arlR*, *sarR*, *sarX*, *rsr*, *codY*, and *sigB*) regulators of *agr* activity was studied by qPCR in the *mroQ* mutant and the parental strain (Fig. 5; see also Table S1 in the supplemental material). Importantly, when these experiments were performed, we observed no significant alteration in the transcription of key *agr* repressors, such as *sigB* (1.1-fold decrease), *sarX* (1.1-fold decrease), *rsr* (1.2-fold decrease), and *codY* (1.2-fold increase). Moreover, although changes of merit were observed for two other *agr* repressors, *arlR* (1.8-fold decrease) and *sarR* (8.2-fold decrease), these were both negative effects and, thus, do not explain the phenotypes observed. When looking at positive regulators of *agr*, we did observe decreased expression for a number of factors, but none at levels that would prove causative to the large decreases in *agr* activity (292-fold decrease in P3 activity in the *mroQ* mutant) thus far observed: *sarA* (3.1-fold decrease), *sarZ* (2-fold decrease), *sarU* (2.1-fold decrease), and *mgrA* (1.9-fold decrease). As such, although the findings are not definitive, it would appear that the positive impact of MroQ on *agr* activity is mediated either by direct interaction or via an as yet unknown regulator of this system.

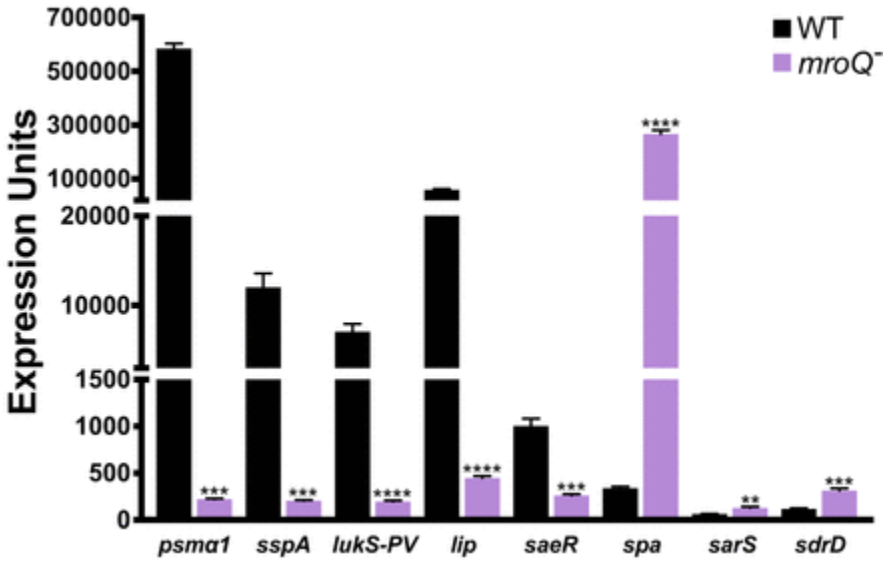

FIGURE 4. The expression of genes regulated by Agr is altered in the *mroQ* mutant. qPCR was performed on the *mroQ* mutant and USA300 wild-type strains grown in TSB to late exponential phase. Expression levels were normalized to the level of 16S rRNA expression. Student's *t* test was used to determine statistical significance. **, $P < 0.01$; ***, $P \leq 0.001$; ****, $P \leq 0.0001$. Error bars show the SEM.

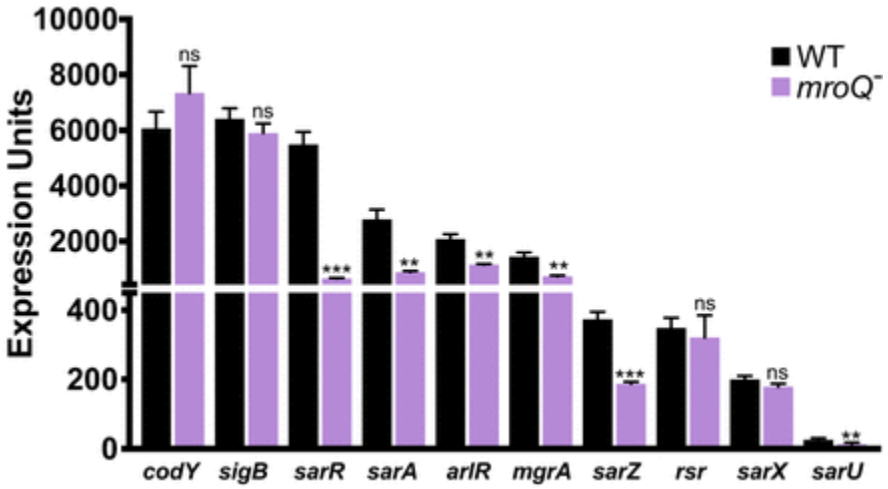

FIGURE 5. Alterations in expression of known regulators of *agr* in the *mroQ* mutant. qPCR was performed on the *mroQ* mutant and USA300 wild-type strains grown in TSB to late exponential phase. Target expression levels were normalized to the level of 16S rRNA expression. Student's *t* test was used to determine statistical significance. **, $P \leq 0.01$; ***, $P \leq 0.001$; ns, not significant. Error bars show the SEM.

Probing the role of MroQ using a global transcriptomic approach. To gain a more global insight into the regulatory effects of MroQ in *S. aureus*, we examined the transcriptome using RNA sequencing (RNA-seq) analysis on our USA300 *mroQ* mutant and its parental strain. A genomic map was created to demonstrate the changes in the transcriptome between the *mroQ* mutant and the parent, as well as the fold changes in gene expression, denoted by a heat map (Fig. 6A). Upon analysis, we found that expression of 123 genes/small RNAs (sRNAs) was

decreased in the *mroQ* mutant, and 109 were increased at a level of ≥3-fold (Fig. 6B; Table S2). Importantly, these studies confirmed our previous data, demonstrating that all components of the Agr system were indeed downregulated in the *mroQ* mutant, with the largest decreases being observed in its two-component system, AgrC (21.6-fold) and AgrA (22.2-fold). When changes were clustered ontologically, the most downregulated group was genes for virulence factors, with 28 genes being decreased in expression in the mutant (Fig. 6C). Furthermore, our previous data regarding virulence factor expression were supported, with significant changes being observed for proteases, toxins, and surface-associated proteins. For example, decreased expression was observed for the phenol-soluble modulins (PSMs) (695-fold), *lukS-PV* (63.5-fold), *sspA* (47-fold), and *scpA* (10-fold) in the mutant strain When looking at the microbial surface component recognizing adhesive matrix molecules (MSCRAMMs), *sdrD* and *spa* demonstrated 5.2-fold and 58.1-fold increases in transcription, respectively, in our *mroQ* mutant.

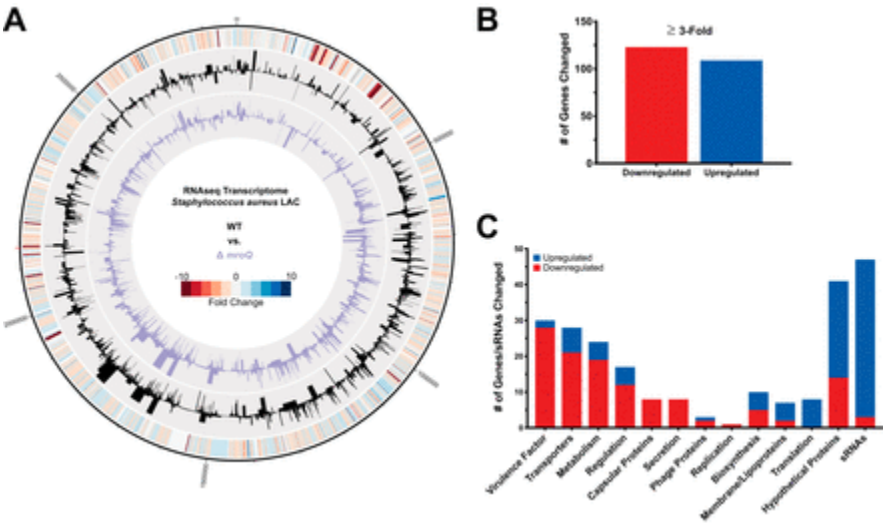

FIGURE 6. *mroQ* disruption produces a global alteration in *S. aureus* gene expression. RNA-seq was performed on the USA300 wild type and its *mroQ* mutant strain. Cultures were grown in TSB to late exponential phase in biological triplicate. RNA was isolated, and the total RNA of replicates was processed for sequencing on an Ion Torrent PGM system. (A) A genomic map was created to denote changes in the *mroQ* mutant transcriptome (inner circle, purple) compared to the wild-type transcriptome (middle circle, black). The outermost circle is a heat map demonstrating fold changes in expression. (B, C) Depiction of the number of genes upregulated and downregulated (B), which were sorted into ontological groups based on known or predicted function (C).

Considering the clear evidence indicating decreased Agr activity in the *mroQ* mutant and the fact that the most profound changes observed in transcription were for virulence determinants, we next examined a full *agr* operon knockout using RNA-seq analysis. A genomic map was created to demonstrate the changes in the transcriptome between the *agr* mutant and the wild type, as well as the fold changes in gene expression via a heat map (Fig. 7A). Implementation of a 3-fold cutoff demonstrated that the expression of 222 genes/sRNAs was decreased and that the expression of 262 was increased in the *agr*-null strain (Fig. 7B; Table S3). When reviewed ontologically, the cluster of genes that appeared to be the most downregulated was, again, genes for virulence factors (Fig. 7C). Upon comparing the *mroQ* mutant transcriptome to that of the

agr mutant, we found a 55% similarity in altered genes and sRNAs (Fig. S1). Of these 129 shared genes, a quarter of them encode virulence factors. It is important to note that the percentage of shared genes/sRNAs is likely higher between the two mutants, as numerous genes identified in the *mroQ* mutant data set are known to be regulated by Agr; however, due to parameters implemented during analysis, they were not present in the *agr* mutant data set because they were expressed at levels too low to be detected upon deletion of *agr*. Additionally, although there were numerous genes whose expression was changed only in the *mroQ* mutant transcriptome, >60% encode hypothetical proteins, thus hampering their functional exploration. To validate the findings for both transcriptome studies, we performed qPCR analysis on a random selection of genes (Table S4), with each showing changes that reproduce those seen in our RNA-seq data sets.

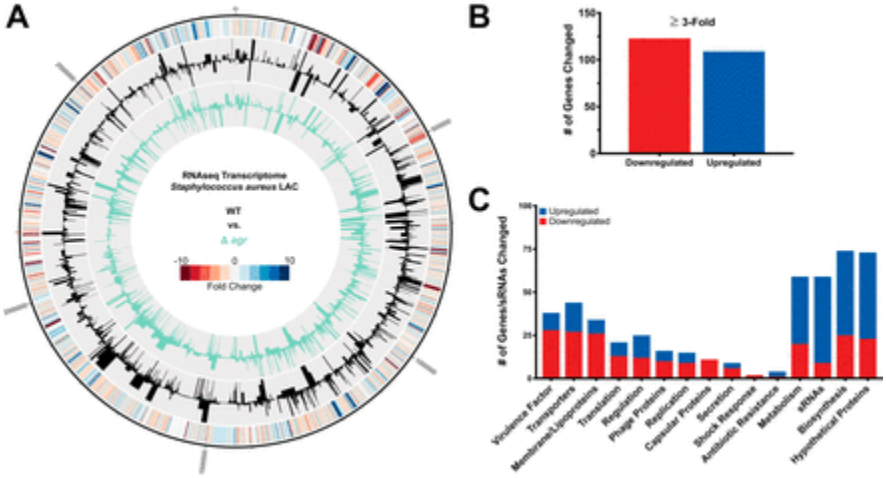

FIGURE 7. Transcriptomic profiling of an *agr* operon deletion mutant. RNA-seq was performed on the USA300 wild type and its *agr* mutant strain. Cultures were grown in TSB to late exponential phase in biological triplicate. RNA was isolated, and the total RNA of replicates was processed for sequencing on an Ion Torrent PGM system. (A) A genomic map was created to denote changes in the *agr* transcriptome (inner circle, green) compared to the wild-type transcriptome (middle circle, black). The outermost circle is a heat map demonstrating fold changes in expression. (B, C) Depiction of the number of genes upregulated and downregulated (B), which were sorted into ontological groups based on known or predicted function (C).

Collectively, the profound similarity in transcriptomes again suggests that mutation of *mroQ* elicits an *agr* mutant-like phenotype. It is important to note, however, that ablated MroQ activity elicits an intermediate *agr*-deficient phenotype, rather than a complete null effect. This is evidenced through a comparison of the fold changes in expression for primary virulence factors between the *mroQ* and *agr* mutants (Table 1), where *mroQ* disruption results in less profound changes in expression than *agr* deletion.

Mutation of *mroQ* enhances biofilm formation. Given the noted increase in the abundance of surface proteins and the marked decrease in virulence factor activity in our *mroQ* mutant strain, we hypothesized that *mroQ* disruption would lead to enhanced biofilm formation, as seen with *agr* mutant strains (32). Using the classic crystal violet assay for biofilm formation, previously described by ourselves and others (33), we determined that the *mroQ* mutant strain did indeed produce a more robust biofilm than our USA300 wild-type strain, with the levels

being similar to those for an *agr* mutant (Fig. 8). This effect was restored to wild-type biofilm formation levels following complementation with *mroQ* in *trans*. These results are consistent with those previously seen for *agr* mutants in multiple different *S. aureus* backgrounds (32, 34).

TABLE 1. Comparison of genes/sRNAs demonstrating changes in expression in both *mroQ* and *agr* mutant RNA-seq data sets

	Fold change in expression	
Gene/sRNA	***mroQ* mutant**	***agr* mutant**
RNAIII gene	−338.2	−162,355.9
splA	−903.1	−1,409.3
lukS-PV	−63.5	−150.2
sspA	−47.5	−90.47
splB	−44.0	−129.1
splE	−43.8	−97.2
lukF-PV	−43.1	−104.8
hlb (*SAUSA300_1918*)	−25.2	−64.7
cap5D	−21.2	−56.0
cap5B	−11.1	−27.5
lukB	−9.8	−21.4
lukA	−9.4	−28.4
ear	−9.0	−82.4
cap5F	−4.6	−11.1
scinA	−3.3	−19.1
saeR	−3.1	−8.0
sdrD	+5.23	+10.2
spa	+58.1	+242.2
SAUSA300s097	+79.5	+164.2

Disruption of *mroQ* leads to an *agr*-mediated decrease in staphyloxanthin production and impaired tolerance to oxidative stress. During our work with the *mroQ* and *agr* mutant strains, we observed that both appeared to have a decrease in the characteristic golden pigment produced by *S. aureus* (Fig. 9A). Due to the importance of staphyloxanthin in protecting *S. aureus* against reactive oxygen species, we performed oxidative stress assays with our collection of strains (Fig. 9B) alongside a *sigB*-null mutant as a pigment-lacking control. Accordingly, strains were exposed to hydrogen peroxide (H_2O_2) at a concentration of 20 mM for 30 min. Following this, the number of CFU per milliliter was determined and compared to that in the inoculum, producing the percent recovery for each strain. As expected, the *sigB* knockout strain demonstrated only 0.18% survival under these conditions, while the wild-type strain produced 20.9% recovery. The *mroQ* mutant demonstrated 3.0% recovery in comparison to our parental strain, while the *agr* mutant demonstrated 2.5% recovery. Importantly, complementation of the *mroQ* mutant resulted in wild-type levels of survival under these conditions. These findings indicate that, in accordance with decreased staphyloxanthin production, the *mroQ* and *agr* mutants both demonstrated reduced tolerance to oxidative stress.

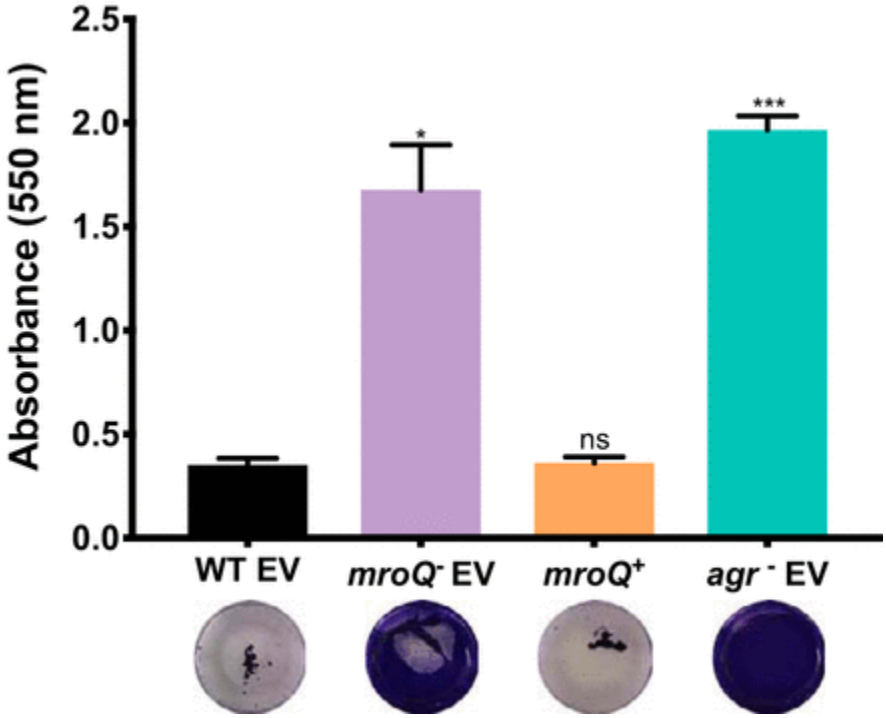

FIGURE 8. The *mroQ* mutant demonstrates an increased capacity for biofilm formation. Strains were grown in 24-well plates in TSB medium containing 5% human plasma. Biofilm formation was quantified with crystal violet staining, followed by extraction with 100% ethanol and OD_{550} measurement. Assays were performed in biological triplicate and technical duplicate. Student's *t* test was used to determine statistical significance. *, $P < 0.05$; ***, $P \leq 0.001$; ns, not significant. Error bars show the SEM. EV, empty vector.

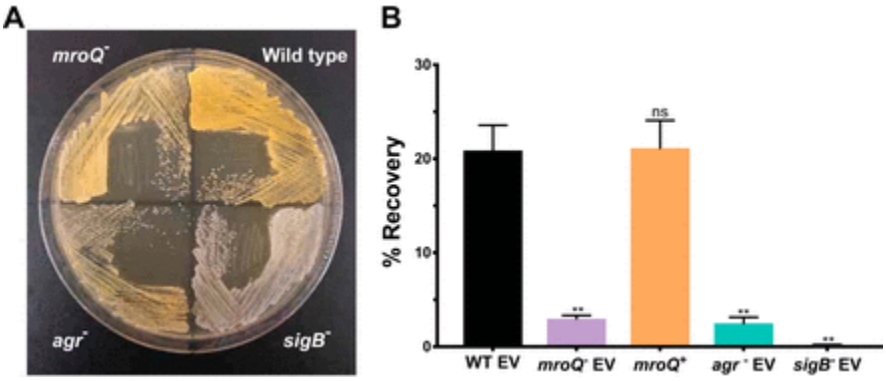

FIGURE 9. Staphyloxanthin production and tolerance to oxidative stress are decreased in the *mroQ* mutant in an *agr*-dependent manner. (A) The strains indicated were streaked onto TSA and grown overnight. (B) Percent recovery of strains following 30 min exposure to H_2O_2 at a 20 mM concentration. Student's *t* test was used to determine statistical significance. **, $P \leq 0.01$; ns, not significant. Error bars show the SEM. EV, empty vector.

MroQ elicits protease-dependent control of Agr activity. As previously discussed, Abi-domain proteins also belong to the M79 metalloprotease family (25, 27, 35). These enzymes are defined by several conserved motifs, with the primary one being a catalytic dyad comprised of neighboring glutamic acid residues (Fig. S2) (25). Thus far, the conserved protease residues of

Abi-domain proteins have not been demonstrated as having essential roles in their function in previous studies involving Gram-positive bacteria (27, 30). As such, we sought to investigate the importance of proteolytic activity for MroQ in exerting its Agr-modulating effects. To do this we created a catalytically inert complementing strain, where the proteolytic residues were converted from glutamic acid to alanine (E141A/E142A) (Fig. S3A). Upon introducing this construct into the *mroQ* mutant strain, we found that this site-directed mutant complement did not restore proteolytic or hemolytic activity to *S. aureus* (Fig. 1A and 2A), demonstrating levels equivalent to those in the *mroQ* and *agr* mutant strains. As such, these results indicate that MroQ is the first Gram-positive bacterial Abi protein to be dependent on its proteolytic capacity for function.

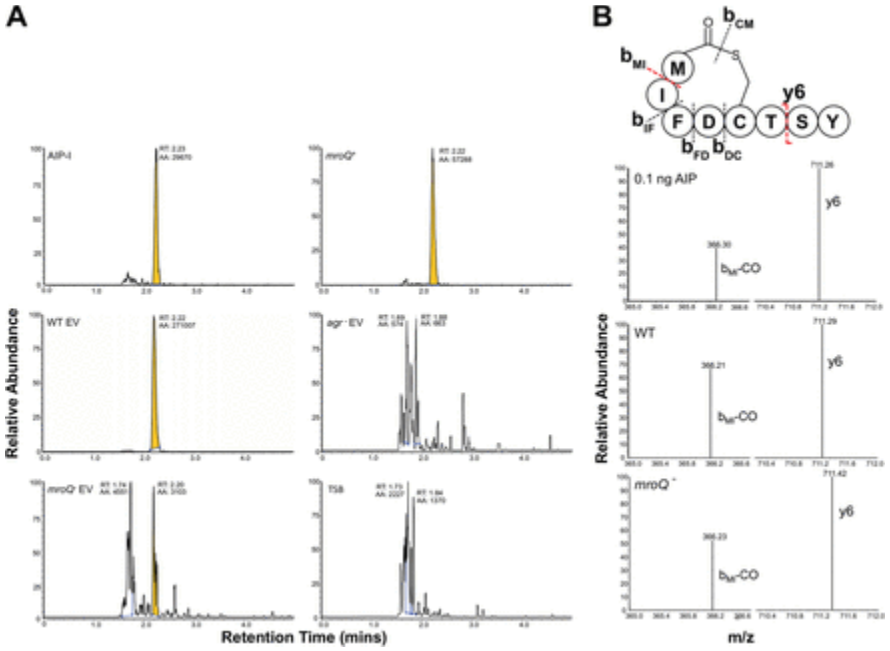

FIGURE 10. Despite impaired *agr* activity, the *mroQ* mutant still produces fully mature AIP. Culture supernatants from the wild type, the *mroQ* mutant, the *agr* mutant, and the *mroQ*-complemented strain, alongside sterile TSB with or without purified AIP-I, underwent UPLC-MS/MS analysis. Experiments were performed three times for each condition, with the chromatograms and spectra shown here proving representative. (A) Chromatograms showing the elution of peptides matching the AIP standard are presented. Peaks at a retention time (RT) of 2.20 to 2.23 min highlighted in yellow correspond to mature AIP-I, and for all conditions, peaks with ~100% relative abundance are labeled with the RT and the peak area (AA). (B) MS/MS spectra comparing the relative abundance of the MRM transitions (*m/z* 961.3 to 711.2 and 365.9) at a retention time of ~2.20 min for the 0.1-ng/ml AIP-I standard, wild type (WT), and *mroQ* mutant shown below a schematic of AIP-I, with the transitions indicated by dotted red lines. The first enables liberation of the y6 ion of AIP (calculated *m/z* 711.30), while the second fragments the cyclic part of AIP, b_{MI}, a prevalent fragment of the cyclic component of AIP (calculated *m/z* 366.23). EV, empty vector.

The presence of mature AIP in *mroQ* mutant supernatants indicates that it plays no role in the processing of AgrD. Given that MroQ controls *agr* activity in a protease-dependent manner and that a central component of the Agr system (the AgrD pheromone precursor) is subject to proteolytic processing, we set out to explore whether MroQ is required for AIP maturation. As

such, we used ultraperformance liquid chromatography (UPLC)-tandem mass spectrometry (MS/MS) analysis to identify mature AIP in the culture supernatants of our various strains. In so doing, we observed AIP-I (retention time [RT] = 2.20 to 2.23 min) in culture supernatants for the wild type, *mroQ* mutant, and *mroQ*-complemented strains but not in the *agr* mutant or in the tryptic soy broth (TSB) blank control (Fig. 10A). Importantly, when analyzing fragmentation patterns, the expected fragments of AIP-I (36) were also observed in supernatants of the wild type and *mroQ* mutant (Fig. 10B) but not in those of the *agr*-null strain. Next, the area under the curve (AA) of AIP peaks in Fig. 10A, in conjunction with an AIP-I standard curve, was used to calculate the AIP-I concentrations in the various culture supernatants (36) (Table S5). Although the level of the *mroQ* mutant was below the lower threshold for accurate quantification (0.1 ng/ml), extrapolation analysis suggested that the level of secretion of mature AIP-I was ~50-fold lower in the mutant than in the wild type (AA = 260,301 and 3,224 for the wild type and the *mroQ* mutant, respectively).

As such, it appears that MroQ does not exert its protease-dependent effects on *agr* activity via direct processing of AgrD or by preventing the proteolytic activity of AgrB (or SpsB, which is also required for AgrD cleavage [37, 38]).

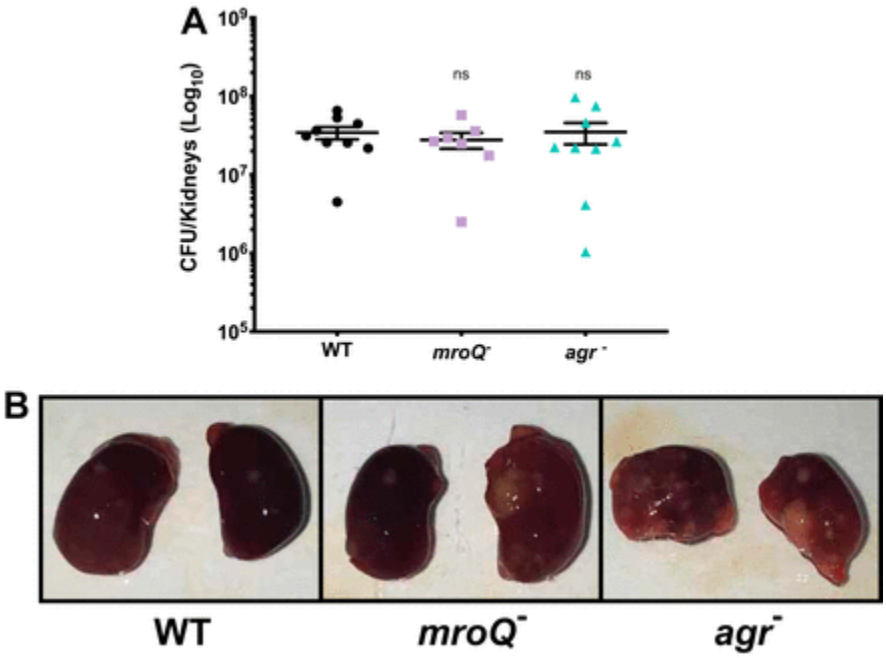

FIGURE 11. Mutation of *mroQ* results in increased renal abscess formation. Female 6-week-old CD-1 mice were injected with the strains shown, and infections were allowed to proceed for 7 days. Following the infection period, mice were sacrificed and the kidneys were harvested. (A) Organs were homogenized in 1 ml of PBS, serially diluted, and plated on TSA to determine the bacterial burden. A Mann-Whitney test was used to determine statistical significance. ns, not significant. (B) Representative images of kidneys harvested from mice infected with the strains noted.

MroQ plays an important role during abscess formation in both localized and systemic infections. Using murine models of infection, we compared the virulent capacity of the *mroQ* and *agr* mutants alongside that of our wild-type strain in systemic and localized

infections. Upon assessing the mortality of mice infected with each strain during a murine model of sepsis and dissemination, we observed no overall difference in survival across the three strains (data not shown). This is perhaps not surprising, given that the *agr* system has previously been shown to have a limited role in influencing this kind of infectious capacity (4, 39). Interestingly, however, we noted that although the kidneys of mice infected with both mutant strains had no alteration in bacterial burden (Fig. 11A), they had an increase in abscess formation (Fig. 11B). Although this finding is curious, it has previously been shown that a defective Agr system results in the increased production of surface factors that are important to abscess formation while, at the same time, limits the production of secreted factors required for dissemination from the abscess (40). As such, this would explain why the *mroQ* mutant demonstrates an increase in renal abscess formation compared to that of the wild type, which mirrors, albeit to a lesser extent, that of a complete *agr* deletion strain.

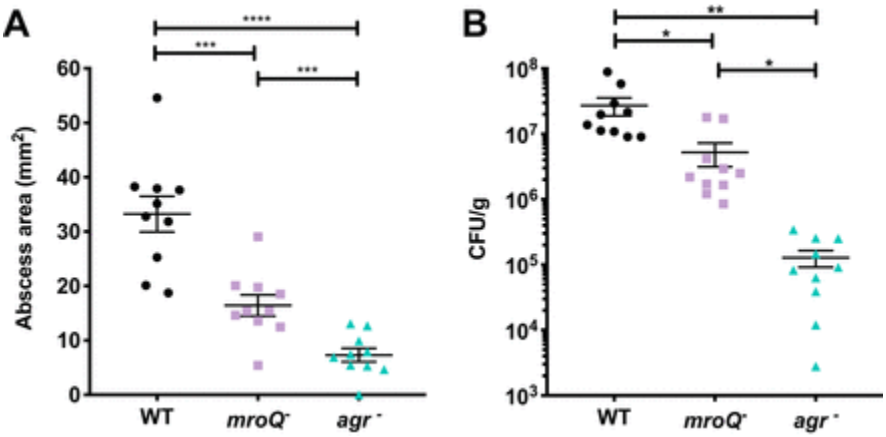

FIGURE 12. The *mroQ* mutant demonstrates attenuated virulence in a murine abscess model of skin infection. Female 6-week-old BALB/c mice were injected subcutaneously, and infections were allowed to proceed for 7 days. (A) Abscesses were measured (width and height), and the area was calculated. (B) The bacterial burden was determined for each abscess. Student's *t* test was used to determine statistical significance. *, $P < 0.05$; **, $P \leq 0.01$; ***, $P \leq 0.001$; ****, $P \leq 0.0001$. Error bars show the SEM.

Skin and soft tissue infections (SSTIs) are commonly caused by *S. aureus*, particularly by USA300 isolates, which are the predominant cause of SSTIs in the United States (41). The success of community-acquired methicillin-resistant *S. aureus* (CA-MRSA) strains in causing SSTIs is a result of their overproduction of important virulence factors (Hla, PSMs, secreted proteases) arising from a hyperactive Agr system (42). To investigate the requirement for MroQ in this kind of localized infection, we next used a murine model of subcutaneous abscess formation with our collection of strains. Following the 7-day infection period, mice were sacrificed, abscesses were excised and measured, and the bacterial burden was determined for each abscess. Upon measuring the abscess area (in square millimeters), the *mroQ* mutant had a 2-fold decrease in comparison to that for the wild type, while the *agr* mutant had a 4.5-fold decrease (Fig. 12A). Additionally, the *mroQ* mutant demonstrated decreased bacterial recovery in the abscess model (5.2-fold decrease) compared to the parent, and although this decrease was significant, it was not at the same magnitude as that in the *agr* mutant (212.2-fold decrease) (Fig. 12B). Finally, the *mroQ* mutant presented decreased levels of dermonecrosis compared to the parental strain, while the *agr* mutant produced no detectable areas of dermonecrosis at all (Fig.

S4). This finding is perhaps to be expected, given that this kind of pathology has previously been shown to heavily depend on Agr-regulated factors (41, 43). Collectively, *mroQ* disruption results in attenuated virulence and dermonecrosis in models of localized skin infection that likely arise from impaired, although not ablated, Agr activity within this strain.

DISCUSSION

Numerous factors have, to date, been identified as playing a role in the regulation of Agr activity, including transcription factors, antisense RNAs, and host factors (5, 8, 20, 22, 23, 44). In this study, we characterized a novel Abi-domain protein and its previously unidentified role as a novel regulator of Agr. While exploring the impact of MroQ on *agr* function, we examined the expression of numerous known regulators of the *agr* system (Fig. 13), including activators and repressors (5, 20, 45). In sum, only one substantial alteration was observed among the collected repressors, which was for *sarR* transcription, although this change was, in fact, a decrease rather than upregulation. Regarding activators, some Sar-family member proteins, including MgrA and SarA, did demonstrate decreased expression; however, these effects were only ~2- to 3-fold in magnitude. As such, the lack of significant changes observed in key repressors and activators does not appear to explain the substantial decreases observed in Agr activity upon *mroQ* disruption. These findings suggest that the influence of MroQ on Agr activity likely occurs through direct interaction with Agr proteins or through as yet unknown effectors of the system.

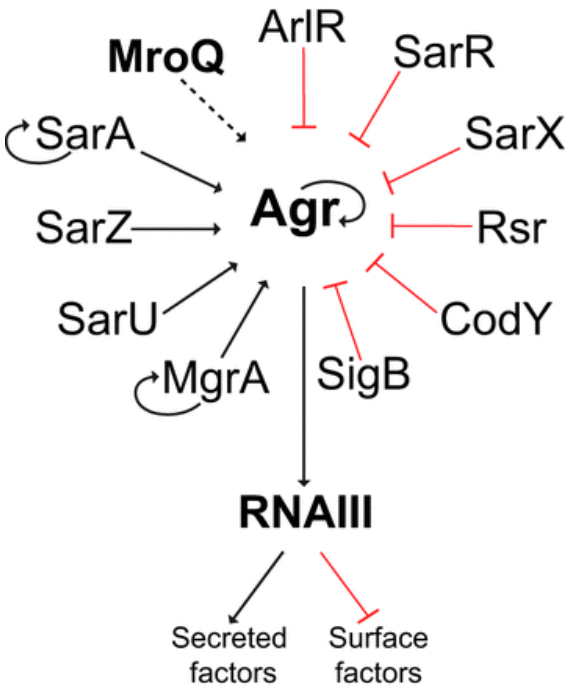

FIGURE 13. Regulatory map illustrating known direct regulators of Agr activity. A map of *agr* regulators was developed based on the literature. Changes in expression of these regulators do not correlate with the substantial decrease in Agr activity observed upon *mroQ* disruption. MroQ appears to directly interact with Agr, resulting in a downstream effect on virulence factor production. Black arrows indicate activation, the red crossbar indicates repression, and the black dashed arrow indicates putative activation.

How such a direct effect could be mediated is perhaps suggested by existing literature on other bacterial Abi proteins. In the first of two recent accounts characterizing Abi-domain proteins in Gram-positive bacteria, a protein called Abx1 was found to have a role in virulence gene expression in *Streptococcus agalactiae* (27). Using a two-hybrid study, it was revealed that Abx1 interacts with the CovS histidine kinase, seemingly via the transmembrane domains of this protein (27). Of note, this interaction was not dependent on the proteolytic activity of Abx1, as mutation of its conserved Glu-Glu residues did not affect its function toward the CovRS system. This study represented a first of its kind, elucidating a novel function for Abi-domain proteins in Gram-positive bacteria. More recently, another Abi-domain protein was characterized in *S. aureus* (30). Here, Poupel et al. investigated SpdC, a membrane protein involved in an interaction network controlling the coordination of division with cell envelope metabolism and host interactions (30). In this study, it was determined that SpdC interacts with 10 different histidine kinases, with several interactions being through their transmembrane domains, similar to the findings in group B streptococci (27). Importantly, SpdC is one of the three Abi proteins in *S. aureus* (see Fig. S1 in the supplemental material) to lack the conserved EE catalytic residues, once again showing that proteolytic activity is not essential for its HK-regulating role.

Thus far, our findings suggest that MroQ may interact directly with the Agr system to modulate its activity. The *mroQ* gene is encoded by a region ~4 kb upstream of the *agr* operon and is expected (as with other Abi proteins) to specify a membrane protein. Importantly, when we performed localization studies for MroQ, we did indeed find that it is present only in membrane fractions (Fig. S3B). At this time, we have yet to confirm potential partners of the interaction for MroQ; however, considering the growing evidence demonstrating that Abi-domain proteins in Gram-positive pathogens interact with and regulate histidine kinases (27, 30), we suggest that MroQ could perhaps mediate its function through AgrC. We note that the Agr system also encodes another membrane protein, AgrB, and that this protein itself also functions as a protease (processing the AgrD pheromone precursor). Our data at this time do not, however, implicate AgrB as the target of MroQ. Specifically, our analysis of culture supernatants by mass spectrometry detected the presence of mature AIP produced by the *mroQ* mutant. As such, this would suggest that MroQ has no role in directly processing AgrD and is not required for AgrB to function correctly. Similarly, we believe that it is unlikely that MroQ is involved in processing AgrA, as AgrC-AgrA interactions have been extensively studied through various crystallization, biochemical, and biophysical studies and do not appear to need adapter proteins to engage (46).

How MroQ might interact with its target(s) within the *S. aureus* cell is currently unclear, but it is seemingly dependent on its proteolytic activity. Members of the M79 peptidase family in eukaryotes typically cleave C-terminal tripeptides from isoprenylated proteins (47), with known substrates including Ras and Ras-related GTP-binding proteins and protein kinases (48). The latter category again provides a link between Abi/M79 proteins and kinase enzymes, further suggesting that AgrC may indeed be the target of MroQ. Determining if the C terminus of AgrC is subject to proteolysis for correct function is an important consideration for continued exploration of MroQ and its role within the *S. aureus* cell.

Using RNA-seq analysis, we found that the entire *agr* system was downregulated in our *mroQ* mutant, with the most substantial decreases being observed for *agrC* and *agrA*, encoding the two-component system. When comparing this data set to a similar transcriptome generated with

an *agr* operon deletion mutant, we observed 55% similarity in the transcriptomes between the two strains, with 25% of these changes corresponding to virulence factors. Of note, a large number of these virulence factors, although they were substantially altered in the *mroQ* mutant, were changed to a much greater degree in the *agr* mutant (Table 1). This is seen on a greater scale when observing trends in virulence factor production, where proteolytic and hemolytic activity was decreased but not completely diminished in the *mroQ*-null strain, as well as in virulence with our murine model of skin infection. Given that *mroQ* mutation phenocopies, but does not completely replicate, the act of *agr* deletion, we suggest that this protein is necessary, but not sufficient, for Agr activity in *S. aureus*.

A singular concern presents itself in the context of our suggestion that mutation of *mroQ* creates a diminished but not abrogated *agr* phenotype: that our phenotype might arise from the fact that we used a mutational insertion strain rather than a deletion mutant. We are supported by the observation that, although there have been screens performed to uncover *S. aureus* mutants that result in ahemolytic phenotypes (49), MroQ has not been identified to date. However, to explore this more fully, we reviewed our *mroQ* mutant RNA sequencing data set and determined that transposon insertion successfully terminates the *mroQ* transcript at the point of insertion (Fig. S5).

In the context of our virulence studies, we made a striking observation when considering the gross pathology presented in the kidneys of mice using a sepsis model. Here, abscess frequency and severity were increased in the *mroQ* mutant and were increased to an even greater level in the *agr*-null strain. At first this might seem contradictory; however, when one explores the literature regarding *S. aureus* abscess formation, this becomes more logical. Specifically, it is known that the early phases of abscess formation are largely dependent on Agr-repressed surface factors, such as Spa, SdrD, ClfA, and Coa. Furthermore, the later stages of infection are characterized by the rupturing of the abscess to elicit dissemination, a process known to be dependent on Agr-activated factors, such as secreted toxins and proteases (2, 50, 51). Accordingly, a defect in quorum sensing, as observed in the *mroQ* mutant, locks abscess formation in the early stages, preventing development to later phases, which are characterized by necrosis and dissemination to new sites (43). The finding that this is more severe in the *agr* mutant than in the *mroQ*-null strain is again in line with our notion that MroQ is a factor that contributes to Agr activity but is not the only factor doing so.

As previously mentioned, models for skin infection are often used to represent SSTIs, which are commonly caused by USA300 strains (52). A key hallmark of subcutaneous skin infections by such strains is dermonecrosis, which presents as necrosis of the epidermis and dermis and which has previously been shown to heavily depend on the Agr-regulated factors alpha-hemolysin (Hla) and phenol-soluble modulins (PSMs) (41, 43, 53). Importantly, our *mroQ* mutant demonstrated decreased promoter activity for *hla* (3.7-fold decrease), although not to the level of an *agr* mutant (6.4-fold decrease). These transcription-based findings directly translate into virulence-based outcomes, as the dermonecrosis presented by the *mroQ* mutant, although reduced compared to that presented by the wild type, was not absent, as was seen for the *agr* mutant. Similarly reduced-but-not-ablated findings for the *mroQ* mutant were presented from our study of abscess size and bacterial load per abscess, where, again, the *agr* mutant was profoundly impaired in its pathogenic potential compared to the parent.

Agr-related factors also play a role in biofilm formation largely identical to that which they play in abscess formation, which explains why *agr*-defective strains demonstrate increased formation of biofilms (51). Biofilms undergo a cycle comprised of three stages: initial attachment, maturation, and dispersal (51, 54). During the initial attachment, adhesin proteins play a crucial role in attachment to an abiotic or biotic surface, as well as in the maturation phase, where they are important for cell-cell adhesion. Conversely, the dispersal of biofilms is highly dependent on enzymes, such as proteases and nucleases, produced by the bacteria to break down components of the biofilm matrix, ultimately allowing for the continuation of the biofilm life cycle from planktonic cells (51). Our *mroQ* mutant demonstrated excellent initial attachment and maturation, likely due to its increased production of MSCRAMMs; however, it failed to properly disperse due to decreased Agr activity and, therefore, decreased the production of secreted enzymes necessary for breaking down the extracellular matrix (51).

In summary, this study identifies MroQ, a novel transmembrane protein, as having a critical role in the regulation of virulence factor production via modulation of the *agr* quorum-sensing system. Further studies are required in order to elucidate the mechanism by which modulation occurs and, more specifically, to identify the MroQ partner(s) of the interaction. Moreover, we must determine how proteolysis is necessary to the function of MroQ, especially considering that this is the first characterized Abi-domain protein to demonstrate protease-dependent activity. In addition, four other Abi-domain proteins exist in *S. aureus*, SAUSA300_0932, SAUSA300_2405, SpdA, and SpdB, the last two of which have been shown to have a role in surface protein regulation (35). Given that surface protein display is under the control of several TCSs in *S. aureus* (55–57), it is entirely possible that they may function by interaction with HKs as well. Accordingly, the continued characterization of MroQ and the complete set of Abi-domain proteins in *S. aureus* remains a focus of study in the Shaw laboratory.

MATERIALS AND METHODS

Reagents, media, and growth conditions. All bacterial strains and plasmids utilized in this study are listed in Table 2. Bacterial strains were grown at 37°C with shaking at 250 rpm. *S. aureus* bacterial strains were grown in tryptic soy broth (TSB) or on tryptic soy agar (TSA), while *Escherichia coli* was grown in lysogeny broth (LB) or on LB agar. TSB supplemented with 5% human plasma was utilized for biofilm experiments. Some investigations required the use of antibiotics for selection, which were added at the following concentrations for *S. aureus*: erythromycin and tetracycline, 5 μg/ml; lincomycin, 25 μg/ml; and chloramphenicol, 10 μg/ml. For *E. coli* strains, ampicillin was used at a concentration of 100 μg/ml. When necessary, X-Gal (5-bromo-4-chloro-3-indolyl-β-d-galactopyranoside) was utilized at a concentration of 40 μg/ml. The induction of complementation was achieved using 0.4 μM cadmium chloride ($CdCl_2$) to induce protein expression. Throughout this study, strains were grown overnight, followed by a 1:100 dilution into fresh TSB and additional growth for 3 h. Strains were then standardized to the optical density at 600 nm (OD_{600}) required for each experiment (detailed below).

TABLE 2. Strains and plasmids used in this study

Strain or plasmid	Genotype/properties[a]	Reference or source
Strains		
E. coli DH5α	Cloning strain	67
S. aureus		
RN4220	Restriction-deficient strain	Lab stock
AH1263	USA300 LAC CA-MRSA Erm^s	68
NE1262	USA300 JE2 *mroQ*::Tn::Erm, *mroQ* mutant	31
USF2299	USA300 LAC *mroQ*::Tn::Erm, *mroQ* mutant	This study
SMM2502	USA300 LAC *mroQ*::Tn::Tet, *mroQ* mutant	This study
SH1001	SH1000 *agr*::Tet, *agr* mutant	61
SMM2601	USA300 LAC *agr*::Tet, *agr* mutant	This study
MJH502	SH1000 *sigB*::Tet, *sigB* mutant	61
SMM2602	USA300 LAC *sigB*::Tet, *sigB* mutant	This study
LES02	SH1000/pAZ106::*aur-lacZ* (Erm^r)	60
SMM2584	USA300 LAC/pAZ106::*aur-lacZ* (Erm^r)	This study
SMM2585	USA300 LAC *mroQ*::Tn::Tet/pAZ106::*aur-lacZ* (Erm^r), *mroQ* mutant	This study
SMM2586	USA300 LAC *agr*::Tet/pAZ106::*aur-lacZ* (Erm^r), *agr* mutant	This study
JLA371	SH1000/pAZ106::*hla-lacZ* (Erm^r)	61
SMM2529	USA300 LAC/pAZ106::*hla-lacZ* (Erm^r)	This study
SMM2530	USA300 LAC *mroQ*::Tn::Tet/pAZ106::*hla-lacZ* (Erm^r), *mroQ* mutant	This study
SMM2531	USA300 LAC agr::Tet/pAZ106::*hla-lacZ* (Erm^r), *agr* mutant	This study
SMM2506	USA300 LAC *mroQ*::Tn::Tet/pJB67::*mroQ*, *mroQ*$^+$	This study
SMM2507	USA300 LAC *mroQ*::Tn::Tet/pJB67::*mroQ*-His$_6$, *mroQ*$^+$	This study
SMM2508	USA300 LAC *mroQ*::Tn::Tet/pJB67::*mroQ*-E141A/E142A, *mroQ*$^+$ catalytically inert mutant	This study
SMM2509	USA300 LAC pEPSA5, LAC WT empty vector	This study
SMM2510	USA300 LAC *mroQ*::Tn::Tet/pEPSA5, *mroQ* mutant empty vector	This study
SMM2511	USA300 LAC *agr*::Tet/pEPSA5, *agr* mutant empty vector	This study
SMM2516	USA300 LAC *mroQ*::Tn::Tet/pEPSA5::*mroQ*, *mroQ*$^+$	This study
SMM2591	USA300 LAC pJB67, LAC WT empty vector	This study
SMM2592	USA300 LAC *mroQ*::Tn::Tet/pJB67, *mroQ* mutant empty vector	This study
SMM2593	USA300 LAC *agr*::Tet/pJB67, *agr* mutant empty vector	This study
SMM2594	USA300 LAC *sigB*::Tet/pJB67, *sigB* mutant empty vector	This study
Plasmids		
pTET	Plasmid for tetracycline resistance cassette switch via allelic exchange and homologous recombination	31
pJB67	pCN51 with optimized RBS and Cd-inducible promoter, Amp^r Erm^r	59
pSMM01	pJB67::*mroQ*	This study
pSMM02	pJB67::*mroQ*-E141A/E142A	This study
pSMM03	pJB67::*mroQ*-His$_6$	This study
pEPSA5	Xylose inducible shuttle vector, Amp^r Cam^r	69
pSMM04	pEPSA5::*mroQ*	This study

[a] Erm, erythromycin; Tet, tetracycline; Amp, ampicillin; Cam, chloramphenicol; RBS, ribosome binding site.

Mutant strain construction. A *mroQ* mutant was obtained from the Nebraska Transposon Mutant Library (NTML) (31). The USA300 JE2 *SAUSA300_1984* transposon mutant was used to create a phage lysate using the phi11 bacteriophage (ϕ11), which was subsequently transduced into the *S. aureus* USA300 LAC background and confirmed by PCR using gene-specific primers (Table 3). Antibiotic resistance cassette switching for the *mroQ* mutant, from erythromycin to

tetracycline, was achieved via allelic exchange and homologous recombination, as described by Bose and coworkers (31). These manipulations were again confirmed via PCR, followed by transduction into a clean USA300 LAC background (and a subsequent round of PCR confirmation). Additionally, the SH1000 *agr* and SH1000 *sigB* mutants were used to create phage lysates for transduction into the *S. aureus* USA300 LAC background.

TABLE 3. Primers used in this study

Primer	Sequence[a]	Description[b]
OL398	TCCTACGGGAGGCAGCAGT	F 16S rRNA
OL399	GGACTACCAGGGTATCTAATCCTGTT	R 16S rRNA
OL1184	AGCCGACCTGAGAGGGTGA	F 16S rRNA qPCR
OL1185	TCTGGACCGTGTCTCAGTTCC	R 16S rRNA qPCR
OL1232	CGCCACATATCCTGATCTTCCAGA	R pAZ106 screening primer
OL2123	GAGTTGTTATCAATGGTCAC	F *sarA* qPCR
OL2124	ACTGCTTTAACAACTTGTGG	R *sarA* qPCR
OL2483	CGGCTTCATTCAAAGTC	F *spa* qPCR
OL2484	GTGCTTGAGATTCGTTTA	R *spa* qPCR
OL2487	TAGTGGTCCATCAACAG	F *lukS-PV* qPCR
OL2488	ACGTTCTACTTCACTGATA	R *lukS-PV* qPCR
OL2495	AACAATCGGATTTAGTACAG	F *sarS* qPCR
OL2496	GTAAGTATTACGCTCATCAA	R *sarS* qPCR
OL2536	AGTTTGCCACGTATCTT	F *agrB* qPCR
OL2537	TTAGCTAAGACCTGCATC	R *agrB* qPCR
OL2540	TTAAGGAAGGAGTGATTTC	F RNAIII gene qPCR
OL2541	GTTCACTGTGTCGATAAT	R RNAIII gene qPCR
OL3116	ACCACAATAACTCAAATTCCTTAATACG	F *saeR* qPCR
OL3117	GTTGAACAACTGTCGTTTGATGA	R *saeR* qPCR
OL3166	CGCGAACGAGAAATCATACAATG	F *sigB* qPCR
OL3167	TCTCTGAAGTCGTGATACATGC	R *sigB* qPCR
OL3612	GGTCCTTTATTA*GCAGCA*TATGTATTCAG	F E141A/E142A site-directed mutagenesis
OL3613	CTGAATACATA*TGCTGC*TAATAAAGGACC	R E141A/E142A site-directed mutagenesis
OL3749	GTAGTTGTAGGTAAAGATACTC	F *sspA* qPCR
OL3750	CCATTTGGATAATTGTCTTG	R *sspA* qPCR
OL3777	ATGgaattcTTA**GTGGTGGTGGTGGTGGTG**TGGAATAAAAATGTGATATATAAAATTCGC	R *mroQ* 6×His tag
OL4011	CTAGGTGAATATGCTGCTACAG	F *codY* qPCR
OL4012	CCATTGTAATAGCAGCTTTATCG	R *codY* qPCR
OL4047	GCTCAAAGACAAGTTAATCGCTAC	F *mgrA* qPCR
OL4048	CGTTTACAGGAGATTCATCCCA	R *mgrA* qPCR
OL4049	CAAAGTTGCTGGGCTTGATTAC	F *arlR* qPCR
OL4050	TTTGTGGCTGACGACGTAAA	R *arlR* qPCR
OL4051	TTCGAACACGTGAAGAGAAAGA	F *sarZ* qPCR
OL4052	CTGATGCTTCTCGTTCTGAAATG	R *sarZ* qPCR
OL4053	CGGTAAAGAATTGAGGGATACATTACAT	F *sarV* qPCR
OL4054	CTTGTCTTTCATCCGTTTCAGAAC	R *sarV* qPCR
OL4055	CGATGAAGCATTGCAAAGATGA	F *sarX* qPCR
OL4056	GTCCTACTTAAATCTAGCTCATCCA	R *sarX* qPCR

Primer	Sequence[a]	Description[b]
OL4093	GGCAGATAATGATGATCGC	F pJB67 MCS
OL4094	CATGTCAACGATAATACAAAATATAATAC	R pJB67 MCS
OL4139	ATGcccgggATGACAAGATTATGGGCATCATTGC	F *mroQ* for pJB67
OL4140	ATGgaattcCATGCTATTCTTATTTGTAAAGCGAAATAAAAA	R *mroQ* for pJB57
OL4332	ATGgaattcATGACAAGATTATGGGCATCATTGC	F *mroQ* for pEPSA5
OL4333	ATGggatccCATGCTATTCTTATTTGTAAAGCGAAATAAAAA	R *mroQ* for pEPSA5
OL4358	CTCGGACCGTCATAAAAAATTTATTTGC	F pEPSA5 MCS
OL4359	CGGCGTTTCACTTCTGAGTTCGGCATGG	R pEPSA5 MCS
OL4445	AACTGTTCTTTCGTCTTGTAAACT	F *sarR* qPCR
OL4446	TGCTCAGAGTTCAAACCTTACT	R *sarR* qPCR
OL4545	TCACCAGTAGAACCAACAAAGG	F *lip* qPCR
OL4546	GTAACGTTGCTACTGCACTACT	R *lip* qPCR
OL4547	GGTATCATCGCTGGCAT	F *psmα1* qPCR
OL4548	TTTACCAGTGAATTGTTCGATTAAG	R *psmα1* qPCR
OL4620	GTATCAAGTTCAAGGTGAGAAT	F *rsr* qPCR
OL4621	GGCCATTCATATCTACATTCATA	R *rsr* qPCR
OL4622	TAGAGACCCACATGATAGTA	F *sarT* qPCR
OL4623	GTTTCATTAATATTTATTTCACTCA	R *sarT* qPCR
OL4624	CAGTTACTCCAATACAACGTAAA	F *sarU* qPCR

[a] Restriction sites are noted by underlined lowercase letters. Italics denotes site-directed mutations. Bold indicates an included hexahistidine tag.
[b] F, forward; R, reverse.

Complementation of the *mroQ* mutation. An *mroQ*-complementing PCR fragment was created using primers OL4139 and OL4140 (all primers used are listed in Table 3), with the former being located immediately at the *mroQ* start codon and the latter being located 88 bp downstream of the 3′ end of the coding region. We also performed site-directed mutagenesis to create a catalytically inert complementing fragment, using splicing by overhang extension (SOE) PCR techniques as previously described by us (58). This was generated using primers OL4139/OL3613 and OL3612/OL4140, where OL3612 and OL3613 contained mutated nucleotide sequences that change the native GAAGAA sequence encoding two glutamic acid residues to a GCAGCA sequence encoding two alanine residues. To facilitate Western blot analysis, a hexahistidine (6×His) tag was added to primer OL4140, creating OL3777, which was used along with OL4139 to create a tagged fragment for localization studies. Each of these three *mroQ* fragments was separately cloned into pJB67, a multicopy plasmid with a $CdCl_2$-inducible promoter and ribosome binding site (59). An additional *mroQ*-complementing strain was created using primers OL4332 and OL4333, which are identical to primers OL4139 and OL4140, with the exception of the presence of different restriction sites that were compatible with pEPSA5, a xylose-inducible shuttle vector.

All constructs were transformed into chemically competent *E. coli* (DH5α) cells, with clones being confirmed using gene-specific primers, followed by Sanger sequencing (Eurofins MWG Operon). Plasmids bearing the correct sequence were transformed into *S. aureus* RN4220 by electroporation and confirmed by PCR. Following this, a phage lysate was created using ϕ11, which was subsequently used to transduce the *S. aureus* USA300 LAC *mroQ* mutant. Strains were confirmed via Sanger sequencing using plasmid-specific primers. Additionally, the pJB67 empty vector was transformed into *S. aureus* RN4220 by electroporation and confirmed by PCR.

A phage lysate was created using ϕ11, which was then used to transduce the *S. aureus* USA300 LAC wild type, USA300 LAC *mroQ* mutant, USA300 LAC *agr* mutant, and USA300 LAC *sigB* mutant, to serve as negative controls. Strains were subsequently confirmed via PCR with plasmid-specific primers OL4093 and OL4094. These control strains were also created with the pEPSA5 empty vector, as described above, and confirmed via PCR with plasmid-specific primers OL4358 and OL4359.

Construction of *lacZ*-reporter fusion strains. *hla-lacZ* and *aur-lacZ* fusion strains were previously constructed using plasmid pAZ106 (60, 61). Phage lysates were created from SH1000 pAZ106::*aur-lacZ* and SH1000 pAZ106::*hla-lacZ* strains using ϕ11, before transducing both separately into the USA300 LAC wild type, alongside its *mroQ* and *agr* mutant strains. Following this, strains containing fusions were confirmed via PCR using a reverse primer located downstream of the multiple-cloning site (MCS) and within the *lacZ* gene, OL1232, and the fusion's respective forward primer.

β-Galactosidase assays. The levels of β-galactosidase activity for the *aur-lacZ* and *hla-lacZ* fusions were quantified as described previously (60). Assays were performed in biological triplicate and technical duplicate. Strains were grown as described above and standardized to an OD_{600} of 0.05. Samples were taken every hour for 6 h and processed using 4-methylumbelliferyl beta-d-galactopyranoside (4-MUG) as a substrate. Student's *t* test with Welch's correction was used to determine statistical significance.

Zymogram and Western blot analysis. Zymograms were performed as previously described (60), using culture supernatants from strains grown for 15 h. The OD_{600}s of these cultures were standardized to the lowest value among the collection, before being concentrated using Amicon Ultra-2 centrifugal 3-kDa filter units (Millipore Sigma). For Western blot analysis, overnight bacterial cultures were grown in biological triplicate as described above, standardized to an OD_{600} of 0.05, and grown to the appropriate time points. Secreted (5 h) and insoluble (3 h) protein fractions were harvested as previously described (62) before being run on 12% SDS-PAGE gels. Samples were subsequently blotted to polyvinylidene difluoride membranes as previously described (33). Immunoblotting was performed with an anti-protein A mouse monoclonal primary antibody (SPA-27; Sigma-Aldrich) or an anti-LukS-PV mouse monoclonal primary antibody (IBT) overnight at 4°C. The secondary antibody used was horseradish peroxidase (HRP)-conjugated goat anti-mouse IgG (Cell Signaling Technologies). For localization studies, the *mroQ*-6×His-complemented strain was grown overnight in biological triplicate as described above. Next, 1 ml of bacterial culture was centrifuged, and supernatants were collected and concentrated overnight using 10% trichloroacetic acid (TCA), with the pellet being processed as previously described (62) to harvest the various protein fractions (cytoplasmic and membrane). Samples were prepared for immunoblotting as described above, and immunoblotting was performed using anti-6×His oligoclonal rabbit primary antibody (Thermo Fisher Scientific) overnight at 4°C. The secondary antibody used was HRP-conjugated goat anti-rabbit IgG (Cell Signaling Technologies). HRP activity was assessed using the SuperSignal West Pico Chemiluminescent substrate (Thermo Fisher Scientific) and visualized on X-ray film.

Hemolysis assay. Overnight bacterial cultures were grown in biological triplicate as described above and standardized to an OD_{600} of 0.05. Cultures were incubated for 6 h before being centrifuged, and the supernatant was removed and mixed (1:1) with hemolysin buffer (0.145 M NaCl, 20 mM $CaCl_2$), followed by the addition of 25 µl whole human blood (BioIVT). Samples were incubated for 40 min at 37°C on a rotator, before being centrifuged at 5.5 × *g* for 1 min. Supernatants were collected and hemolysis was determined by measuring the OD_{543} using a BioTek Synergy II plate reader and 96-well plates. Student's *t* test with Welch's correction was used to determine statistical significance.

qPCR analysis. Quantitative real-time PCR (qPCR) was performed on samples isolated at hour 5 in biological triplicate as previously described (63). Various targets were examined, and their levels of expression were normalized to that of 16S rRNA (the primers used are listed in Table 3). Student's *t* test with Welch's correction was used to determine the statistical significance of the expression units.

Transcriptomic analysis via RNA sequencing. RNA-seq was performed as previously described (64). Briefly, cultures of the USA300 LAC wild type, alongside its *mroQ* and *agr* mutant strains, were standardized and grown in biological triplicate for 5 h using the growth method described above. Next, 5 ml of each culture was immediately combined with 5 ml of ice-cold phosphate-buffered saline (PBS) and pelleted by centrifugation at 4°C, and the supernatant was removed. Total RNA was isolated using an RNeasy kit (Qiagen), with the DNA removed using a Turbo DNA-free kit (Ambion). DNA removal was confirmed by PCR using primers OL398 and OL399, and RNA quality was assessed using an Agilent 2100 bioanalyzer and an RNA 6000 Nano kit (Agilent) to confirm integrity; samples with an RNA integrity number (RIN) of greater than 9.7 were used. Biological replicates were pooled at equal RNA concentrations, before rRNA depletion using a Ribo-Zero kit for Gram-positive bacteria (Illumina) and a MICROBExpress bacterial mRNA enrichment kit (Ambion). The removal efficiency was confirmed, again using an Agilent 2100 bioanalyzer and RNA 6000 Nano kit. Strand-specific library preparation was performed using a total RNA-seq kit (v2) and whole-transcriptome protocol (Ion Torrent). Sample libraries were assessed for quality, concentration, and average fragment size using the Agilent 2100 bioanalyzer and a high-sensitivity DNA kit (Agilent). Prepared fragment libraries were ligated to Ion Sphere particles, amplified, and enriched using an Ion Torrent personal genome machine (OT2 200) kit and Ion OneTouch 2 system. Particles were then sequenced using an Ion 318 (v2) chip (Ion Torrent).

Bioinformatics. Raw data (.fasta) files were exported from the Ion Torrent PGM system server using the File Exporter plug-in and uploaded to the Qiagen Bioinformatics Workbench for analysis. Reads corresponding to rRNA were filtered, removed by aligning to known rRNA sequences, and discarded. Unmapped (filtered) read sequences were aligned to the USA300 FPR3757 reference genome (GenBank accession number NC_007793.1), and expression values were calculated using the RNA-Seq Analysis function. Experimental comparisons were carried out following quantile normalization by use of the RNA-seq experimental fold change feature. Expression values calculated for each gene are shown as normalized reads per kilobase per million values.

Biofilm formation assay. The ability of our strains to form biofilms was examined using methods previously described (33). Overnight bacterial cultures were grown in biological triplicate as described above and standardized to an OD_{600} of 0.5. Cultures were then seeded in a 24-well plate containing TSB, 5% human plasma, and erythromycin for plasmid retention in technical duplicate and grown for 24 h. Following incubation, the biofilms were washed with PBS and briefly fixed with 100% ethanol. The biofilms were then allowed to dry overnight prior to staining with crystal violet for 15 min. Following this, the wells were washed to remove excess crystal violet and allowed to dry overnight. Biofilm formation was quantified by extracting crystal violet stain with 100% ethanol and measuring the OD_{550} using a BioTek Synergy II plate reader. Student's *t* test with Welch's correction was used to determine statistical significance.

Oxidative stress assay. Overnight bacterial cultures were grown in biological triplicate as described above and standardized to an OD_{600} of 0.1. Samples were treated with 20 mM hydrogen peroxide for 30 min with shaking at 37°C. After this time, the reaction was stopped by the addition of 10 μg/ml catalase. Percent recovery was determined by comparing the number of CFU per milliliter preexposure to the number of CFU per milliliter postexposure. Student's *t* test with Welch's correction was used to determine statistical significance.

Murine model of sepsis and dissemination. The murine model of sepsis and dissemination was performed as previously described (65). Briefly, 6-week old, female CD-1 mice were purchased from Charles River Laboratories and allowed to acclimate for 1 week prior to the start of experimentation. Wild-type and mutant strains were grown as described above and standardized to an OD_{600} of 0.05. Cultures were grown overnight for 15 h on three separate days, and the average number of CFU per milliliter across replicates was calculated for each strain. This average number of CFU per milliliter was used to determine the volume of bacteria needed to obtain a 10-ml inoculum of 5×10^8 ($[5 \times 10^8$/average CFU/ml$] \times 10$ ml). On the day of infection, appropriate aliquots from fresh overnight cultures prepared in the same way were centrifuged, resuspended in 1 ml sterile PBS to wash, centrifuged once more, and finally, resuspended in a total volume of 10 ml sterile PBS. Next, 100 μl of the bacterial suspension was administered via tail vein injection, providing a final inoculum of 5×10^7 CFU/ml. Infections were monitored over a 7-day period or until the mice reached a premoribund state, at which point they were euthanized (65). At this time, kidneys were harvested and stored at −80°C. These were subsequently photographed before being homogenized in 1 ml PBS and serially diluted onto TSA to determine the bacterial burden (number of CFU per milliliter). A Mann-Whitney test was performed to determine statistical significance for the bacterial burden in kidneys.

Murine model of skin abscess formation. The murine model of skin abscess formation was performed as described previously (66). Briefly, wild-type and mutant strains were grown for 2.5 h until reaching an OD_{600} of approximately 0.75. Bacterial cells were centrifuged, and the pellet was resuspended in sterile PBS for inoculation. Inocula were prepared at 1×10^7 CFU/50 μl for injections and subsequently confirmed via serial dilution and plating. Six-week-old BALB/c female mice were shaved on the right flank prior to treatment with Nair for full hair removal. Subsequently, mice were injected in the right flank with 50 μl, and infections were allowed to persist for 7 days. Throughout the infection period, the mice were monitored for irregular activity or distress. Following the 7-day infection period, mice were euthanized and the

abscesses were excised, weighed, and measured (length and width) to determine the abscess area (in square millimeters). The abscesses were then homogenized, and homogenates were diluted and plated onto TSA to determine the bacterial burden (number of CFU per gram). Student's *t* test with Welch's correction was used to determine statistical significance.

Mass spectrometry of culture supernatants for AIP-I detection. The wild-type, *mroQ* mutant, *agr* mutant, and pEPSA5::*mroQ* -complemented strains were grown for 15 h in TSB supplemented with 1% xylose as described above. The cultures were pelleted, and the supernatants were filter sterilized (pore size, 0.2 μm) to ensure that they were cell free. Samples were then processed by the Triad Mass Spectrometry Facility at The University of North Carolina—Greensboro, alongside controls of TSB and purified AIP-I (AnaSpec Inc., Fremont, CA). Samples were analyzed using an Acquity UPLC (Waters, Milford, MA) coupled to a TSQ Quantum Access triple-quadrupole mass spectrometer (Thermo, San Jose, CA) with a heated electrospray ionization (HESI) source. A 5-μl injection of each sample was eluted from an Acquity BEH C_{18} column (2.1 mm by 50 mm, 1.8-μm-particle-size packing) using a binary solvent system consisting of Optima-grade water and Optima-grade acetonitrile (both containing 0.1% formic acid) at a flow rate of 300 μl/min. The gradient initiated at 75:25 water-acetonitrile and increased linearly to 50:50 water-acetonitrile over 3.5 min. The column was then washed with 100% acetonitrile and reequilibrated to starting conditions. The mass spectrometer was operated in multiple-reaction-monitoring mode using positive ion electrospray ionization. Transitions of *m/z* 961.3 ($[M+H]^+$) to *m/z* 711.2 and *m/z* 961.3 to *m/z* 365.9 were monitored at a gas pressure of 1.5 and a collision energy of 29 and 43, respectively. Quantitative analysis was performed using the *m/z* 961.3-to-711.2 transition. The HESI source was operated using the following parameters: tube lens offset, 198 V; spray voltage, 5.00 kV; sheath gas pressure, 60; auxiliary gas pressure, 35; capillary temperature, 200°C; and capillary offset, 35 V.

Ethics statement. All animal work was performed under the approval of the University of South Florida's Institutional Animal Care and Use Committee (IACUC) and Ohio University's IACUC by trained lab personnel.

Accession number(s). Experimental data from this study were deposited in the NCBI Gene Expression Omnibus (GEO) database (GEO accession number GSE121625).

Supplemental material. Supplemental material for this article may be found at https://doi.org/10.1128/IAI .00002-19.

ACKNOWLEDGMENTS

This work was supported in part by grants AI080626 and AI124458 (both to L.N.S.) from the National Institute of Allergy and Infectious Diseases and by grant AT006860 from the National Center for Complementary and Integrative Health (to N.B.C. and D.A.T.).

REFERENCES

1. Balasubramanian D, Harper L, Shopsin B, Torres VJ. 2017. Staphylococcus aureus pathogenesis in diverse host environments. Pathog Dis 75:1ftx005. https://doi.org/10.1093/femspd/ftx005.

2. Cheung AL, Bayer AS, Zhang G, Gresham H, Xiong Y-Q. 2004. Regulation of virulence determinants in vitro and in vivo in Staphylococcus aureus. FEMS Immunol Med Microbiol 40:1–9. https://doi.org/10.1016/S0928-8244(03)00309-2.

3. Foster TJ, Hook M. 1998. Surface protein adhesins of Staphylococcus aureus. Trends Microbiol 6:484 – 488. https://doi.org/10.1016/S0966-842X(98)01400-0.

4. Thomer L, Schneewind O, Missiakas D. 2016. Pathogenesis of Staphylococcus aureus bloodstream infections. Annu Rev Pathol 11:343–364. https://doi.org/10.1146/annurev-pathol-012615-044351.

5. Reyes D, Andrey DO, Monod A, Kelley WL, Zhang G, Cheung AL. 2011. Coordinated regulation by AgrA, SarA, and SarR to control agr expression in Staphylococcus aureus. J Bacteriol 193:6020–6031. https://doi.org/10.1128/JB.05436-11.

6. Ballal A, Ray B, Manna AC. 2009. sarZ, a sarA family gene, is transcriptionally activated by MgrA and is involved in the regulation of genes encoding exoproteins in Staphylococcus aureus. J Bacteriol 191:1656–1665. https://doi.org/10.1128/JB.01555-08.

7. Manna AC, Cheung AL. 2006. Expression of SarX, a negative regulator of agr and exoprotein synthesis, is activated by MgrA in Staphylococcus aureus. J Bacteriol 188:4288–4299. https://doi.org/10.1128/JB.00297-06.

8. Fournier B, Klier A, Rapoport G. 2001. The two-component system ArlS-ArlR is a regulator of virulence gene expression in Staphylococcus aureus. Mol Microbiol 41:247–261. https://doi.org/10.1046/j.1365-2958.2001.02515.x.

9. Cheung AL, Schmidt K, Bateman B, Manna AC. 2001. SarS, a SarA homolog repressible by agr, is an activator of protein A synthesis in Staphylococcus aureus. Infect Immun 69:2448 – 2455. https://doi.org/10.1128/IAI.69.4.2448-2455.2001.

10. Clarke SR, Foster SJ. 2006. Surface adhesins of Staphylococcus aureus. Adv Microb Physiol 51:187–224. https://doi.org/10.1016/S0065-2911(06)51004-5.

11. Queck SY, Jameson-Lee M, Villaruz AE, Bach TH, Khan BA, Sturdevant DE, Ricklefs SM, Li M, Otto M. 2008. RNAIII-independent target gene control by the agr quorum-sensing system: insight into the evolution of virulence regulation in Staphylococcus aureus. Mol Cell 32:150 – 158. https://doi.org/10.1016/j.molcel.2008.08.005.

12. Gray B, Hall P, Gresham H. 2013. Targeting agr- and agr-like quorum sensing systems for development of common therapeutics to treat multiple gram-positive bacterial infections. Sensors (Basel) 13:5130–5166. https://doi.org/10.3390/s130405130.

13. Boisset S, Geissmann T, Huntzinger E, Fechter P, Bendridi N, Possedko M, Chevalier C, Helfer AC, Benito Y, Jacquier A, Gaspin C, Vandenesch F, Romby P. 2007. Staphylococcus aureus RNAIII coordinately represses the synthesis of virulence factors and the transcription regulator Rot by an antisense mechanism. Genes Dev 21:1353–1366. https://doi.org/10.1101/gad.423507.

14. Wang B, Zhao A, Novick RP, Muir TW. 2014. Activation and inhibition of the receptor histidine kinase AgrC occurs through opposite helical transduction motions. Mol Cell 53:929 – 940. https://doi.org/10.1016/j.molcel.2014.02.029.

15. Thoendel M, Horswill AR. 2013. Random mutagenesis and topology analysis of the autoinducing peptide biosynthesis proteins in Staphylococcus aureus. Mol Microbiol 87:318 – 337. https://doi.org/10.1111/mmi.12100.

16. George Cisar EA, Geisinger E, Muir TW, Novick RP. 2009. Symmetric signalling within asymmetric dimers of the Staphylococcus aureus receptor histidine kinase AgrC. Mol Microbiol 74:44 –57. https://doi.org/10.1111/j.1365-2958.2009.06849.x.

17. Tamber S, Cheung AL. 2009. SarZ promotes the expression of virulence factors and represses biofilm formation by modulating SarA and agr in Staphylococcus aureus. Infect Immun 77:419–428. https://doi.org/10.1128/IAI.00859-08.

18. Shaw LN, Aish J, Davenport JE, Brown MC, Lithgow JK, Simmonite K, Crossley H, Travis J, Potempa J, Foster SJ. 2006. Investigations into sigmaB-modulated regulatory pathways governing extracellular virulence determinant production in Staphylococcus aureus. J Bacteriol 188:6070–6080. https://doi.org/10.1128/JB.00551-06.

19. Andrey DO, Jousselin A, Villanueva M, Renzoni A, Monod A, Barras C, Rodriguez N, Kelley WL. 2015. Impact of the regulators SigB, Rot, SarA and sarS on the toxic shock Tst promoter and TSST-1 expression in Staphylococcus aureus. PLoS One 10:e0135579. https://doi.org/10.1371/journal.pone.0135579.

20. Roux A, Todd DA, Velazquez JV, Cech NB, Sonenshein AL. 2014. CodY-mediated regulation of the Staphylococcus aureus Agr system integrates nutritional and population density signals. J Bacteriol 196:1184–1196. https://doi.org/10.1128/JB.00128-13.

21. Sterba KM, Mackintosh SG, Blevins JS, Hurlburt BK, Smeltzer MS. 2003. Characterization of Staphylococcus aureus SarA binding sites. J Bacteriol 185:4410–4417. https://doi.org/10.1128/JB.185.15.4410-4417.2003.

22. Fechter P, Caldelari I, Lioliou E, Romby P. 2014. Novel aspects of RNA regulation in Staphylococcus aureus. FEBS Lett 588:2523–2529. https://doi.org/10.1016/j.febslet.2014.05.037.

23. Painter KL, Krishna A, Wigneshweraraj S, Edwards AM. 2014. What role does the quorum-sensing accessory gene regulator system play during Staphylococcus aureus bacteremia? Trends Microbiol 22:676–685. https://doi.org/10.1016/j.tim.2014.09.002.

24. Chopin MC, Chopin A, Bidnenko E. 2005. Phage abortive infection in lactococci: variations on a theme. Curr Opin Microbiol 8:473– 479. https://doi.org/10.1016/j.mib.2005.06.006.

25. Kjos M, Snipen L, Salehian Z, Nes IF, Diep DB. 2010. The Abi proteins and their involvement in bacteriocin self-immunity. J Bacteriol 192:2068–2076. https://doi.org/10.1128/JB.01553-09.

26. Pei J, Grishin N. 2001. Type II CAAX prenyl endopeptidases belong to a novel superfamily of putative membrane-bound metalloproteases. Trends Biomed Sci 26:275–277. https://doi.org/10.1016/S0968-0004(01)01813-8.

27. Firon A, Tazi A, Da Cunha V, Brinster S, Sauvage E, Dramsi S, Golenbock DT, Glaser P, Poyart C, Trieu-Cuot P. 2013. The Abi-domain protein Abx1 interacts with the CovS histidine kinase to control virulence gene expression in group B Streptococcus. PLoS Pathog 9:e1003179. https://doi.org/10.1371/journal.ppat.1003179.

28. Krute CN, Carroll RK, Rivera FE, Weiss A, Young RM, Shilling A, Botlani M, Varma S, Baker BJ, Shaw LN. 2015. The disruption of prenylation leads to pleiotropic rearrangements in cellular behavior in Staphylococcus aureus. Mol Microbiol 95:819–832. https://doi.org/10.1111/mmi.12900.

29. Okada M. 2011. Post-translational isoprenylation of tryptophan. Biosci Biotechnol Biochem 75:1413–1417. https://doi.org/10.1271/bbb.110087.

30. Poupel O, Proux C, Jagla B, Msadek T, Dubrac S. 2018. SpdC, a novel virulence factor, controls histidine kinase activity in Staphylococcus aureus. PLoS Pathog 14:e1006917. https://doi.org/10.1371/journal.ppat.1006917.

31. Fey PD, Endres JL, Yajjala VK, Widhelm TJ, Boissy RJ, Bose JL, Bayles KW. 2013. A genetic resource for rapid and comprehensive phenotype screening of nonessential Staphylococcus aureus genes. mBio 4:e00537-12. https://doi.org/10.1128/mBio.00537-12.

32. Yarwood JM, Bartels DJ, Volper EM, Greenberg EP. 2004. Quorum sensing in Staphylococcus aureus biofilms. J Bacteriol 186:1838 –1850. https://doi.org/10.1128/JB.186.6.1838-1850.2004.

33. Weiss A, Moore BD, Tremblay MH, Chaput D, Kremer A, Shaw LN. 2017. The omega subunit governs RNA polymerase stability and transcriptional specificity in Staphylococcus aureus. J Bacteriol 199:e00459-16. https://doi.org/10.1128/JB.00459-16.

34. Boles BR, Horswill AR. 2008. Agr-mediated dispersal of Staphylococcus aureus biofilms. PLoS Pathog 4:e1000052. https://doi.org/10.1371/journal.ppat.1000052.

35. Frankel MB, Wojcik BM, DeDent AC, Missiakas DM, Schneewind O. 2010. ABI domain-containing proteins contribute to surface protein display and cell division in Staphylococcus aureus. Mol Microbiol 78:238 –252. https://doi.org/10.1111/j.1365-2958.2010.07334.x.

36. Junio HA, Todd DA, Ettefagh KA, Ehrmann BM, Kavanaugh JS, Horswill AR, Cech NB. 2013. Quantitative analysis of autoinducing peptide I (AIP-I) from Staphylococcus aureus cultures using ultrahigh performance liquid chromatography-high resolving power mass spectrometry. J Chromatogr B Analyt Technol Biomed Life Sci 930:7–12. https://doi.org/10.1016/j.jchromb.2013.04.019.

37. Cregg KM, Wilding I, Black MT. 1996. Molecular cloning and expression of the spsB gene encoding an essential type I signal peptidase from Staphylococcus aureus. J Bacteriol 178:5712–5718. https://doi.org/10.1128/jb.178.19.5712-5718.1996.

38. Kavanaugh JS, Thoendel M, Horswill AR. 2007. A role for type I signal peptidase in Staphylococcus aureus quorum sensing. Mol Microbiol 65:780 –798. https://doi.org/10.1111/j.1365-2958.2007.05830.x.

39. Nygaard TK, Pallister KB, Ruzevich P, Griffith S, Vuong C, Voyich JM. 2010. SaeR binds a consensus sequence within virulence gene promoters to advance USA300 pathogenesis. J Infect Dis 201:241–254. https://doi.org/10.1086/649570.

40. Cheng AG, DeDent AC, Schneewind O, Missiakas D. 2011. A play in four acts: Staphylococcus aureus abscess formation. Trends Microbiol 19: 225–232. https://doi.org/10.1016/j.tim.2011.01.007.

41. Malachowa N, Kobayashi SD, Braughton KR, DeLeo FR. 2013. Mouse model of Staphylococcus aureus skin infection. Methods Mol Biol 1031: 109–116. https://doi.org/10.1007/978-1-62703-481-4_14.

42. Thurlow LR, Joshi GS, Richardson AR. 2012. Virulence strategies of the dominant USA300 lineage of community-associated methicillin-resistant Staphylococcus aureus (CA-MRSA). FEMS Immunol Med Microbiol 65:5–22. https://doi.org/10.1111/j.1574-695X.2012.00937.x.

43. Kim HK, Missiakas D, Schneewind O. 2014. Mouse models for infectious diseases caused by Staphylococcus aureus. J Immunol Methods 410:88–99. https://doi.org/10.1016/j.jim.2014.04.007.

44. Beenken KE, Mrak LN, Griffin LM, Zielinska AK, Shaw LN, Rice KC, Horswill AR, Bayles KW, Smeltzer MS. 2010. Epistatic relationships between sarA and agr in Staphylococcus aureus biofilm formation. PLoS One 5:e10790. https://doi.org/10.1371/journal.pone.0010790.

45. Luong TT, Dunman PM, Murphy E, Projan SJ, Lee CY. 2006. Transcription profiling of the mgrA regulon in Staphylococcus aureus. J Bacteriol 188:1899 –1910. https://doi.org/10.1128/JB.188.5.1899-1910.2006.

46. Srivastava SK, Rajasree K, Fasim A, Arakere G, Gopal B. 2014. Influence of the AgrC-AgrA complex on the response time of Staphylococcus aureus quorum sensing. J Bacteriol 196:2876 – 2888. https://doi.org/10.1128/JB.01530-14.

47. Plummer LJ, Hildebrandt ER, Porter SB, Rogers VA, McCracken J, Schmidt WK. 2006. Mutational analysis of the Ras converting enzyme reveals a requirement for glutamate and histidine residues. J Biol Chem 281:4596–4605. https://doi.org/10.1074/jbc.M506284200.

48. Zhang FL, Casey PJ. 1996. Protein prenylation: molecular mechanisms and functional consequences. Annu Rev Biochem 65:241–269. https://doi.org/10.1146/annurev.bi.65.070196.001325.

49. Burnside K, Lembo A, de Los Reyes M, Iliuk A, Binhtran NT, Connelly JE, Lin WJ, Schmidt BZ, Richardson AR, Fang FC, Tao WA, Rajagopal L. 2010. Regulation of hemolysin expression and virulence of Staphylococcus aureus by a serine/threonine kinase and phosphatase. PLoS One 5:e11071. https://doi.org/10.1371/journal.pone.0011071.

50. Gong J, Li D, Yan J, Liu Y, Li D, Dong J, Gao Y, Sun T, Yang G. 2014. The accessory gene regulator (agr) controls Staphylococcus aureus virulence in a murine intracranial abscesses model. Braz J Infect Dis 18:501–506. https://doi.org/10.1016/j.bjid.2014.03.005.

51. Paharik AE, Horswill AR. 2016. The staphylococcal biofilm: adhesins, regulation, and host response. Microbiol Spectr 4:VMBF-0022-2015. https://doi.org/10.1128/microbiolspec.VMBF-0022-2015.

52. David MZ, Daum RS. 2010. Community-associated methicillin-resistant Staphylococcus aureus: epidemiology and clinical consequences of an emerging epidemic. Clin Microbiol Rev 23:616–687. https://doi.org/10.1128/CMR.00081-09.

53. Kennedy AD, Bubeck Wardenburg J, Gardner DJ, Long D, Whitney AR, Braughton KR, Schneewind O, DeLeo FR. 2010. Targeting of alphahemolysin by active or passive immunization decreases severity of USA300 skin infection in a mouse model. J Infect Dis 202:1050 –1058. https://doi.org/10.1086/656043.

54. Archer NK, Mazaitis MJ, Costerton JW, Leid JG, Powers ME, Shirtliff ME. 2011. Staphylococcus aureus biofilms: properties, regulation, and roles in human disease. Virulence 2:445– 459. https://doi.org/10.4161/viru.2.5.17724.

55. Walker JN, Crosby HA, Spaulding AR, Salgado-Pabon W, Malone CL, Rosenthal CB, Schlievert PM, Boyd JM, Horswill AR. 2013. The Staphylococcus aureus ArlRS two-component system is a novel regulator of agglutination and pathogenesis. PLoS Pathog 9:e1003819. https://doi.org/10.1371/journal.ppat.1003819.

56. Montgomery CP, Boyle-Vavra S, Daum RS. 2010. Importance of the global regulators Agr and SaeRS in the pathogenesis of CA-MRSA USA300 infection. PLoS One 5:e15177. https://doi.org/10.1371/journal.pone.0015177.

57. Falord M, Mader U, Hiron A, Debarbouille M, Msadek T. 2011. Investigation of the Staphylococcus aureus GraSR regulon reveals novel links to virulence, stress response and cell wall signal transduction pathways. PLoS One 6:e21323. https://doi.org/10.1371/journal.pone.0021323.

58. Krute CN, Bell-Temin H, Miller HK, Rivera FE, Weiss A, Stevens SM, Shaw LN. 2015. The membrane protein PrsS mimics sigmaS in protecting Staphylococcus aureus against cell wall-targeting antibiotics and DNA-damaging agents. Microbiology 161:1136 –1148. https://doi.org/10.1099/mic.0.000065.

59. Windham IH, Chaudhari SS, Bose JL, Thomas VC, Bayles KW. 2016. SrrAB modulates Staphylococcus aureus cell death through regulation of cidABC transcription. J Bacteriol 198:1114 –1122. https://doi.org/10.1128/JB.00954-15.

60. Shaw L, Golonka E, Potempa J, Foster SJ. 2004. The role and regulation of the extracellular proteases of Staphylococcus aureus. Microbiology 150:217–228. https://doi.org/10.1099/mic.0.26634-0.

61. Horsburgh MJ, Aish JL, White IJ, Shaw L, Lithgow JK, Foster SJ. 2002. sigmaB modulates virulence determinant expression and stress resistance: characterization of a functional rsbU strain derived from Staphylococcus aureus 8325-4. J Bacteriol 184:5457–5467. https://doi.org/10.1128/JB.184.19.5457-5467.2002.

62. Rivera FE, Miller HK, Kolar SL, Stevens SM, Jr, Shaw LN. 2012. The impact of CodY on virulence determinant production in community-associated methicillin-resistant Staphylococcus aureus. Proteomics 12:263–268. https://doi.org/10.1002/pmic.201100298.

63. Miller HK, Carroll RK, Burda WN, Krute CN, Davenport JE, Shaw LN. 2012. The extracytoplasmic function sigma factor sigmaS protects against both intracellular and extracytoplasmic stresses in Staphylococcus aureus. J Bacteriol 194:4342– 4354. https://doi.org/10.1128/JB.00484-12.

64. Carroll RK, Weiss A, Shaw LN. 2014. RNA-sequencing of Staphylococcus aureus messenger RNA. Methods Mol Biol 1373:131–141. https://doi.org/10.1007/7651_2014_192.

65. Kolar SL, Ibarra JA, Rivera FE, Mootz JM, Davenport JE, Stevens SM, Horswill AR, Shaw LN. 2013. Extracellular proteases are key mediators of Staphylococcus aureus virulence via the global modulation of virulence-determinant stability. Microbiologyopen 2:18 –34. https://doi.org/10.1002/mbo3.55.

66. Keogh RA, Zapf RL, Wiemels RE, Wittekind MA, Carroll RK. 2018. The intracellular cyclophilin PpiB contributes to the virulence of Staphylococcus aureus independent of its PPIase activity. Infect Immun https://doi.org/10.1128/IAI.00379-18.

67. Salisbury V, Hedges RW, Datta N. 1972. Two modes of "curing" transmissible bacterial plasmids. J Gen Microbiol 70:443– 452. https://doi.org/10.1099/00221287-70-3-443.

68. Boles BR, Thoendel M, Roth AJ, Horswill AR. 2010. Identification of genes involved in polysaccharide-independent Staphylococcus aureus biofilm formation. PLoS One 5:e10146. https://doi.org/10.1371/journal.pone.0010146.

69. Forsyth RA, Haselbeck RJ, Ohlsen KL, Yamamoto RT, Xu H, Trawick JD, Wall D, Wang L, Brown-Driver V, Froelich JM, C KG, King P, McCarthy M, Malone C, Misiner B, Robbins D, Tan Z, Zhu Zy ZY, Carr G, Mosca DA, Zamudio C, Foulkes JG, Zyskind JW. 2002. A genome-wide strategy for the identification of essential genes in Staphylococcus aureus. Mol Microbiol 43:1387–1400. https://doi.org/10.1046/j.1365-2958.2002.02832.x.